Electrochemical characteristic of non-stoichiometric $SmBa_{0.45}Sr_{0.5}Co_2O_{5+d}$ layered perovskite oxide system for IT-SOFC cathode

Kyeong Eun Song [a, b], Harald Schlegl [c], Hyunil Kang [d], Wonseok Choi [d], Jung Hyun Kim [a,*]

[a] Department of Advanced Materials Science and Engineering, Hanbat National University, 125, Dongseo-Daero, Yuseong-Gu, Daejeon, 34158, Republic of Korea

[b] Fuel Cell Innovations Co., Ltd. 41-7, Techno 11-ro, Yuseong-gu, Daejeon, Republic of Korea

[c] Chemistry Department, Lancaster University, Bailrigg, Lancaster LA1 4YB, United Kingdom

[d] Department of Electrical Engineering, Hanbat National University, 125, Dongseo-Daero, Yuseong-Gu, Daejeon, 34158, Republic of Korea

Corresponding author:*

Jung Hyun Kim: jhkim2011@hanbat.ac.kr, jhkim1870@gmail.com,

Tel: +82-42-821-1239, Fax: +82-42-821-1592,

Department of Advanced Materials Science and Engineering, Hanbat National University, 125, Dongseo-Daero, Yuseong-Gu, Daejeon, 34158, Republic of Korea

Abstract

In this study, the composition of the layered perovskite $SmBa_{0.5}Sr_{0.5}Co_2O_{5+d}$ was changed to different non-stoichiometric compositions by changing the substitution amount of Ba and Sr.

$SmBa_{0.45}Sr_{0.5}Co_2O_{5+d}$ (SBSCO-0.45/0.5) showed the lowest area specific resistance (ASR) because the area % caused by high binding energy (HBE) of O_{1s} in the X-ray photoelectron spectroscopy (XPS) analysis was the largest compared to all other tested compositions and also the unit cell volume was smaller than that of other samples.

The dense $SmBa_{0.5}Sr_{0.48}Co_2O_{5+d}$ (SBSCO-0.5/0.48) showed the highest electrical conductivity. This is because SBSCO-0.5/0.48 has the smallest decrease in oxygen contents compared to other samples when subject to temperature increase. Also, through XPS analysis, it was found that the area % of the Co^{3+} and Co^{4+} coexistence regions of Co_{2p} of SBSCO-0.5/0.48 was the largest. The electrical conductivity values and behaviors of the porous SBSCO-0.45/0.5 and SBSCO-0.5/0.48 were not significantly different.

Comparing the single-cell performance with composite cathodes comprised of SBSCO-0.45/0.5 and SBSCO-0.5/0.48 with CGO91, the results show that the single-cell with the SBSCO-0.45/0.5 and CGO91 cathode showed higher maximum power density.

Keywords: Solid oxide fuel cell, Non-stoichiometric composition cathode, Area specific resistance, Electrical conductivity, Microstructure.

1. Introduction

Recently, an abnormal climate caused by global warming has become a problem worldwide. The main cause of global warming is an increase of the CO_2 concentration in the atmosphere. One of the main causes of CO_2 generation is the use of fossil fuels [1, 2]. Accordingly, the use of a fuel cell was suggested as an alternative way of conversion of chemical energy to electrical energy instead of burning fossil fuels [1-4]. One type of the fuel cells for power generation is the SOFC (Solid oxide fuel cell) in which the cathode, the electrolyte and the anode are all made of ceramic materials [5]. An SOFC has the advantage of high efficiency and output power compared to other fuel cells due to its high operating temperature of 600 ~ 1000 ºC. However, long-term performance degradation occurs in SOFCs due to problems such as chemical reactions between components, Cr poisoning and metal oxidation [6-10].

Since the problems described for the SOFC are caused or worsened by very high operation temperatures, one way to solve these problems could be the conduction of research aiming for the development of on Intermediate Temperature-operating Solid Oxide Fuel Cell (IT-SOFC), operating at a lower temperature range of 500 ~ 800 ºC. Since an IT-SOFC operates at a relatively low temperature, problems of reduced cathode performance caused by slow oxygen reduction reaction (ORR) and activation loss occur [11-13]. The cathode is responsible for about 50 % of total polarization resistance, so it is an important factor determining the overall performance of an SOFC. Therefore, it is necessary to study cathode materials which show fast ORR even in the mid-low temperature range [14-16].

Our research groups recently reported the excellent electrochemical properties of the layered perovskite $SmBa_{0.5}Sr_{0.5}Co_2O_{5+d}$ (SBSCO) as an SOFC cathode. The single phase SBSCO showed an area specific resistance (ASR) value of 0.092 Ωcm^2 at 600 ºC. A composite cathode

comprised of SBSCO and $Ce_{0.9}Gd_{0.1}O_2$ (CGO91) at a ratio of 1:1 showed ASR values of 0.013 Ωcm^2 , which is even lower than the ASR of the single phase SBSCO at same temperature [17].

When a non-stoichiometric composition is applied to the different sites of a layered perovskite (A, $A^{/}$ or B), various changes occur in the electrochemical properties of the layered perovskite. Therefore, our research team conducted a previous study in which a non-stoichiometric composition was applied to the Sm cations situated at the A-site. As a result of this previous study, the $Sm_{0.95}Ba_{0.5}Sr_{0.5}Co_2O_{5+d}$ layered perovskite showed excellent electrochemical properties such as an ASR value of 0.118 Ωcm^2 at 700 ºC and a maximum power density of 2.84 W/cm^2 at 850 ºC [18].

While studies on the non-stoichiometric composition of SBSCO layered perovskite oxide system have not been conducted at other research institutes, this present study investigates perovskites with a non-stoichiometric composition of Ba and Sr cations at the $A^{/}$-site, partially removing these ions caused structural deficiency at the $A^{/}$-site. More specifically, in this study, $SmBa_{0.5-x}Sr_{0.5}Co_2O_{5+d}$, $SmBa_{0.5}Sr_{0.5-x}Co_2O_{5+d}$ and $SmBa_{0.5-x}Sr_{0.5-x}Co_2O_{5+d}$ ($x = 0.01 \sim 0.05$) were selected as non-stoichiometric compositions. Thermal analysis, electrochemical characterization and microscopic microstructure investigation were performed for each of the different compositions of the $A^{/}$-site deficient layered perovskites in this study with the goal to investigate the correlation between the nature and degree of non-stoichiometry on the one side and electrical conductivity and ASR on the other side.

2. Experimental

2. 1. Powder preparation

Sm_2O_3 (99.9%, Alfa aesar), $BaCO_3$ (99.8%, Alfa aesar), $SrCO_3$ (99.8%, Samchun chemicals) and Co_3O_4 (99.7%, Alfa aesar) powders were used for the synthesis of non-stoichiometric

$SmBa_{0.5}Sr_{0.5-x}Co_2O_{5+d}$, $SmBa_{0.5-x}Sr_{0.5}Co_2O_{5+d}$ and $SmBa_{0.5-x}Sr_{0.5-x}Co_2O_{5+d}$ (x=0.01 ~ 0.05) layered perovskite oxide systems by solid state reaction. For each composition the different powders were accurately weighed and mixed using an agate mortar with a pestle and 100 ml ethanol. The powder mixtures were heated to 1000°C using a ramping rate of 5°C/min and calcined for 6 hours at 1000 ºC as a first calcination. After that, a secondary calcination was carried out in an electric furnace heated to 1100 ºC with a ramping rate of 5 ºC/min, holding the calcination temperature for 8 hours.

The abbreviations of the synthetic materials are summarized in Table 1.

Table 1. Abbreviations of $SmBa_{0.5}Sr_{0.5-x}Co_2O_{5+d}$, $SmBa_{0.5-x}Sr_{0.5}Co_2O_{5+d}$ and $SmBa_{0.5-x}Sr_{0.5-x}Co_2O_{5+d}$ (x=0.01 ~ 0.05) layered perovskite oxide systems

Chemical composition	**Abbreviation**	**Chemical composition**	**Abbreviation**
$SmBa_{0.5}Sr_{0.5}Co_2O_{5+d+d}$	SBSO-0.5/0.5	$SmBa_{0.47}Sr_{0.5}Co_2O_{5+d}$	SBSCO-0.47/0.5
$SmBa_{0.5}Sr_{0.49}Co_2O_{5+d}$	SBSCO-0.5/0.49	$SmBa_{0.46}Sr_{0.5}Co_2O_{5+d}$	SBSCO-0.46/0.5
$SmBa_{0.5}Sr_{0.48}Co_2O_{5+d}$	SBSCO-0.5/0.48	$SmBa_{0.45}Sr_{0.5}Co_2O_{5+d}$	SBSCO-0.45/0.5
$SmBa_{0.5}Sr_{0.47}Co_2O_{5+d}$	SBSCO-0.5/0.47	$SmBa_{0.49}Sr_{0.49}Co_2O_{5+d}$	SBSCO-0.49/0.49
$SmBa_{0.5}Sr_{0.46}Co_2O_{5+d}$	SBSCO-0.5/0.46	$SmBa_{0.48}Sr_{0.48}Co_2O_{5+d}$	SBSCO-0.48/0.48
$SmBa_{0.5}Sr_{0.45}Co_2O_{5+d}$	SBSCO-0.5/0.45	$SmBa_{0.47}Sr_{0.47}Co_2O_{5+d}$	SBSCO-0.47/0.47
$SmBa_{0.49}Sr_{0.5}Co_2O_{5+d}$	SBSCO-0.49/0.5	$SmBa_{0.46}Sr_{0.46}Co_2O_{5+d}$	SBSCO-0.46/0.46
$SmBa_{0.48}Sr_{0.5}Co_2O_{5+d}$	SBSCO-0.48/0.5	$SmBa_{0.45}Sr_{0.45}Co_2O_{5+d}$	SBSCO-0.45/0.45

2. 2. X-ray diffraction (XRD) and High temperature-XRD (HT-XRD)

X-ray diffraction (XRD) patterns of the synthesized $SmBa_{0.5}Sr_{0.5-x}Co_2O_{5+d}$, $SmBa_{0.5-x}Sr_{0.5}Co_2O_{5+d}$, and $SmBa_{0.5-x}Sr_{0.5-x}Co_2O_{5+d}$ (x=0.01 ~ 0.05) were obtained on a Model Rigaku/SmartLab (45 Kv, 200 mA, Cu kα radiation) at 10 ~ 90 º (2θ). In order to analyze the crystal structure change and phase stability with respect to the temperature, a high temperature-XRD (HT-XRD) experiment was carried out using $SmBa_{0.45}Sr_{0.5}Co_2O_{5+d}$ (SBSCO-0.45/0.5) powder with the lowest ASR. In case of the HT-XRD, the SBSCO-0.45/0.5 was heated to 5 ºC/min using the Rigaku/SmartLab model, and XRD spectra were obtained within a temperature range of 50 ~ 900 ºC at steps of 100 ºC. The obtained data were analyzed using the MDI JADE 6 software. In addition, the miller indices were found through the obtained XRD data, and the lattice parameters were calculated using the MDI JADE 6 program.

2. 3. Thermal expansion coefficient (TEC) and Thermogravimetric analysis (TGA)

A SBSCO-0.5/0.5 (SBSCO-0.5/0.5) pellet for the measurement of the TEC was prepared in a uniaxial hydraulic press applying a pressure of 2 x 10^3 kg/m^2 to create a rectangular-shaped bar with the dimensions 25 mm x 6 mm x 3 mm. Subsequently this pellet was heated to 1100°C using a ramping rate of 5°C/min and sintered at 1100 ºC for 3 hours. The TEC results of SBSCO-0.5/0.5 were observed using a thermomechanical analyzer of the model NETZSCH/TMA 402 F1 within a temperature range of RT ~ 900 ºC, which is the same temperature range electrical conductivity measurements and ASR measurements were conducted in. Based on the electrical conductivity and ASR results, samples of the compositions SBSCO-0.5/0.48, SBSCO-0.45/0.5, SBSCO-0.45/0.45 and SBSCO-0.46/0.46 were selected for TGA analysis. TGA measurement of each sample was performed using a thermal analysis platform of the model LABSYS Evo within a temperature range of RT ~ 900 ºC.

2. 4. Electrochemical characterization

For the fabrication of the electrolytes, individual samples of 2.5 g of $Ce_{0.9}Gd_{0.1}O_{2-d}$ (CGO91, Rhodia) powder were pressed into disc shapes using a uniaxial hydraulic press at a maximum pressure of 2 x 10^3 kg/m^2. The CGO91 pellets were heated to 1450 ºC with a ramping rate of 5 ºC/min and sintered at this temperature for 6 hours and the final geometry of the sintered pellets was cylindric with approximately 22 mm in diameter and 0.95 mm in thickness. For the cathode inks, samples of approximately 5 g $SmBa_{0.5}Sr_{0.5-x}Co_2O_{5+d}$, $SmBa_{0.5-x}Sr_{0.5}Co_2O_{5+d}$ and $SmBa_{0.5-x}Sr_{0.5-x}Co_2O_{5+d}$ (x=0.01 ~ 0.05) powders fabricated as described in chapter 2.1 were put in a 150 ml Nalgene bottle with 0.1 g of a polyester/polyamide copolymer dispersant of the model KD-1 and 125 ml of acetone, and ball milled for 24 hours. Then, it was mixed with the binder system vehicle (a-Terpineol 95 wt% + Butvar 5 wt%) and stirred at room temperature.

For the composite cathode ink, $SmBa_{0.5}Sr_{0.5-x}Co_2O_{5+d}$, $SmBa_{0.5-x}Sr_{0.5}Co_2O_{5+d}$ and $SmBa_{0.5-x}Sr_{0.5-x}Co_2O_{5+d}$ (x=0.01 ~ 0.05) powders were mixed with CGO91 at a mass ratio of 1:1. After weighing 5 g of the mixed powder, the fabrication of the composite cathode ink was completed using the above-mentioned method. After the prepared inks were applied to the electrolytes using screen printing, samples were heated to 1000 ºC with a ramping rate of 5 ºC/min and sintered for 1 hour. The ASR of the symmetric half-cells were measured using nStat/HS technologies model; the measurements were performed in a frequency range of 0.05 Hz ~ 2.5 MHz in air atmosphere, decreasing the temperature from a starting measurement at 900 ºC to a final measurement at 650 ºC using 50 ºC increments.

2. 5. Conductivity measurements

2. 5. 1. Conductivity measurements of SBSCO with dense microstructure

The $SmBa_{0.5}Sr_{0.5-x}Co_2O_{5+d}$, $SmBa_{0.5-x}Sr_{0.5}Co_2O_{5+d}$ and $SmBa_{0.5-x}Sr_{0.5-x}Co_2O_{5+d}$ (x=0.01 ~ 0.05) pellets for the measurement of electrical conductivity were prepared using a uniaxial hydraulic press applying a maximum pressure of 2 x 10^3 kg/m^2 to create rectangular-shaped bars (25 mm x 6 mm x 3 mm). After that, the pellets were heated to 1100 ºC with a ramping rate of 5 ºC/min and sintered for 3 hours to create sample bars with a dense microstructure.

The electrical conductivities of the dense samples were measured using a DC 4 probe method, connecting the samples to a Keithley 2400 current source meter using Pt wires. Two series of conductivity measurements were performed, one starting measurements at 50 ºC heating up to 900 ºC (Heating cycle in air) in incremental steps of 50 ºC, followed immediately by a second series of measurements, decreasing the temperature in 50 ºC increments from 900 ºC to 50 ºC (Cooling cycle in air) in air atmosphere. For measurements under lower oxygen partial pressure 99.99% N_2 gas (100 cc/min) was fed into the quartz tube used as measurement environment. The electrical conductivity under thin N_2 atmosphere was measured through the same method as measured in air atmosphere by first increasing the temperature from 50 ºC to 900 ºC (Heating cycle in N_2) and subsequently decreasing the temperature from 900 ºC to 50 ºC (Cooling cycle in N_2). Conductivity under different load conditions was investigated applying currents of 0.1 A, 0.5 A and 1 A at each temperature.

2. 5. 2. Conductivity measurements of SBSCO with porous microstructure

Since the cathodes for the actual SOFCs are designed in the form of a porous thick film, a porous microstructural cathode was prepared and compared with a dense cathode. The CGO91 and 8YSZ powders were pressed at 1.5 x 10^3 kg/m^2 into rectangular-shaped metal molds (30 mm x 23 mm x 2 mm) and heated to 1450 ºC with a ramping rate of 5 ºC/min and sintered for 6 hours in air atmosphere to complete a dense CGO91 and a dense 8YSZ pellet. The cathode

inks were applied to the CGO91 and to the 8YSZ pellets using screen printing to fabricate porous microstructural cathodes, these samples were heated to 1000 ºC using a ramping rate of 5 ºC/min and sintered at 1000 ºC for 1 hour [19]. Pt paste was used as an electrical conductor for the electrical conductivity measurement. For this purpose, Pt paste was screen printed onto the cathode in the form of 4 probes to form Pt line circuits to apply current and voltage.

The schematic diagram and abbreviations for the porous cathodes were summarized in Figure 1 and Table 2.

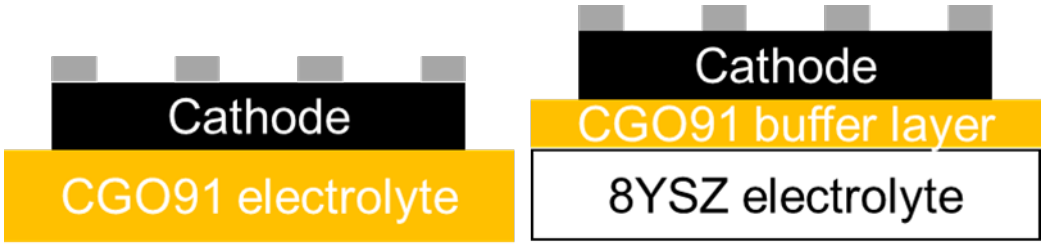

Figure 1. Schematic diagrams of porous cathode

Table 2. Abbreviation of porous cathode samples

Cathode material	**electrolyte**	**Abbreviation**
$SmBa_{0.45}Sr_{0.5}Co_2O_{5+d}$ (SBSCO-0.45/0.5)	8YSZ (Y)	H-0.45/0.5Y
	CGO91 (G)	H-0.45/0.5G
$SmBa_{0.5}Sr_{0.48}Co_2O_{5+d}$ (SBSCO-0.5/0.48)	Y	H-0.5/0.48Y
	G	H-0.5/0.48G

The electrical conductivities of porous samples were measured using a DC 4 probe method connecting them to a Keithley 2400 current source meter using Pt clamp and Pt wires. The conductivities were measured in heating cycle in air, cooling cycle in air, heating cycle in N_2

and cooling cycle in N_2 using the same experimental setup as for the conductivity measurement of the dense cathodes.

Currents of 0.05 A, 0.075 A, 0.1 A and 0.3 A were applied in the air atmosphere and currents of 0.01 A, 0.02 A, 0.03 A, 0.04 A and 0.05 A were applied in the N_2 atmosphere to measure the electrical conductivity under various load conditions.

2. 6. Scanning electron microscopy (SEM)

SEM images were obtained from the very same samples used for the conductivity measurements reported in section 2.5. After completion of the conductivity tests each sample was sputtered with Pt (Platinum), the microstructures of the samples were observed at an acceleration voltage of 10 kV using a SEM (HITACHI SU-5000 model).

2. 7. X-ray photoelectron spectroscopy (XPS)

Based on the results of electrochemical analysis, SBSCO-0.5/0.48, SBSCO-0.45/0.5, SBSCO-0.45/0.45 and SBSCO-0.46/0.46 were selected for XPS analysis. A Thermo VG Scientific/Sigma probe model was used in the XPS experiments and Al Ka radiation (1486.6 eV) was used as the excitation source for the narrow scan and the wide scan. The binding energy of the elements was calibrated with respect to the C_{1s} peak fixed at 284.4 eV. The data was analyzed using the PeakFit version 4 software [20].

2. 8. Single cell test

The single-cell performances of SBSCO-0.45/0.5 and SBSCO-0.5/0.48 composite cathodes were analyzed for power density measurement. Measurement was performed using an anode

supported cell of cylindrical shape in which the YSZ electrolyte was thinly coated (around 2 μm) on top of a NiO/YSZ composite porous anode of 200 μm thickness. To prevent a chemical reaction between YSZ and the cathode, a CGO91 buffer layer with a thickness of around 5 μm was coated onto the cathode side of the YSZ electrolyte using screen printing, and then this combination of anode, electrolyte and buffer layer was heated to 1300 ºC with a ramping rate of 5 ºC/min and sintered at 1300 ºC for 2 hours.

After screen printing of the composite cathode layer on top of the CGO91 buffer layer, heating to 1000 ºC with a ramping rate of 5 ºC/min and sintering for 1 hour completed the SBSCO-0.45/0.5 (NiO-YSZ/YSZ/Buffer layer/SBSCO-0.45/0.5 composite cathode) single-cell and the SBSCO-0.5/0.48 (NiO-YSZ/YSZ/Buffer layer/SBSCO-0.5/0.48 composite cathode) single-cells. H_2 gas (99.99 %, 100 cc/min) was fed into the anode, and air gas (99.99 %, 100 cc/min) was fed into the cathode. The power density was measured at different temperatures by decreasing the temperature from 850 ºC to 600 ºC at 50 ºC steps using a Biologic/SP-240 potentiostat.

3. Results and discussions

3. 1. X-ray diffraction (XRD) analysis of layered perovskite oxide systems

XRD results of $SmBa_{0.5}Sr_{0.5-x}Co_2O_{5+d}$, $SmBa_{0.5-x}Sr_{0.5}Co_2O_{5+d}$ and $SmBa_{0.5-x}Sr_{0.5-x}Co_2O_{5+d}$ (x = 0.01 ~ 0.05) are shown in Figure 2. (a). All cathodes were identified as single-phase layered perovskite structures because typical peaks were found at about 23.0, 33.1, 40.7, 47.1, 59.4, 69.6 and 78.4 º [21, 22]. The peak splittings measured at 23, 47 and 59 º in the XRD diagrams of $SmBa_{0.5}Sr_{0.5-x}Co_2O_{5+d}$, $SmBa_{0.5-x}Sr_{0.5}Co_2O_{5+d}$ and $SmBa_{0.5-x}Sr_{0.5-x}Co_2O_{5+d}$ (x = 0.01 ~ 0.05) oxide systems indicate that their crystalline structure is orthorhombic [22-24].

The calculated lattice parameters and unit cell volumes are summarized in Figure 2. (b) and

Table S1. Lattice parameters of a, b and c-axis were calculated to be in the ranges of 3.851 ~ 3.868, 3.800 ~ 3.818, and 7.636 ~ 7.672 Å, respectively. Changes of these lattice parameters as a consequence of deficiency of different $A^{/}$ site cations can be analyzed as follows.

First, the lattice parameters of a, b, and c-axis of SBSCO-0.5/0.45 with reduced Sr in ① in Figure 2. (b) were 3.860, 3.803, and 7.670 Å, respectively. That shows that as the substitution of Sr decreased, there was no significant change in a and b-axis lattice parameters, but the c-axis lattice parameter increased. The a, b and c-axis lattice parameters of SBSCO-0.45/0.45 in ② in Figure 2. (b) with both reduced Ba and reduced Sr were 3.860, 3.807 and 7.672 Å, respectively, which are similar to the a and b-axis of SBSCO-0.5/0.5. However, as the non-stoichiometric properties increase in the order of SBSCO-0.5/0.5 < SBSCO-0.49/0.49 < SBSCO-0.48/0.48 < SBSCO-0.47/0.47 < SBSCO-0.46/0.46 < SBSCO-0.45/0.45, the c-axis lattice parameters increase. Finally, the a and b-axis lattice parameter of SBSCO-0.45/0.5 in ③ in Figure 2. (b) were similar to SBSCO-0.5/0.5, but the c-axis lattice parameter was 7.636 Å, showing the lowest value for the c-axis among all compositions, even smaller than the c-axis in the SBSCO-0.5/0.5 unit cell.

Among all the compositions, the unit cell volume of SBSCO-0.45/0.45 in Figure 2. (b), which has the largest non-stoichiometric characteristics, was the largest. In addition, in SBSCO-0.45/0.5 with the largest decrease of Ba substitution, the unit cell volume was confirmed to be the smallest.

This distinction can be explained as stemming from the difference in ionic radii of Ba and Sr substituted into the $A^{/}$-site in the chemical composition of $AA^{/}B_2O_{5+d}$; the ionic radius of Ba^{2+} (1.60 Å) is considerably larger than that of Sr^{2+} (1.27 Å). When considering a crystal in which

Ba and Sr are substituted into the layered structure, it has a structure in which [Ln-O] and [$A^{/}$-O] layers appear along the c-axis. As a result, Sr can replace Ba at the $A^{/}$-site when the substitution amount of Ba decreases. The distance between the [Ln-O] layer and the [A/-O] layer decreases; these relationships result in decreased c-axis lattice parameter and the unit cell volume also decreases [25-27].

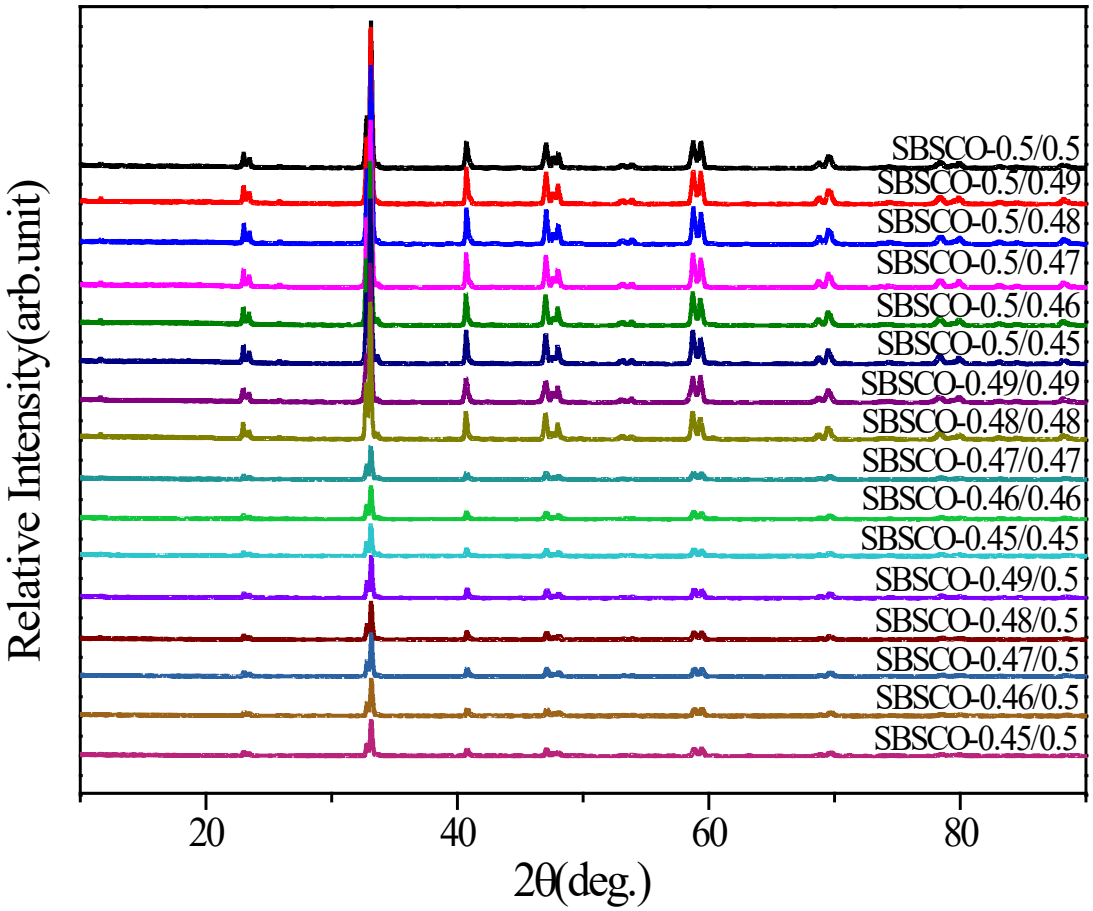
Relative Intensity(arb.unit)
SBSCO-0.5/0.5
SBSCO-0.5/0.49
SBSCO-0.5/0.48
SBSCO-0.5/0.47
SBSCO-0.5/0.46
SBSCO-0.5/0.45
SBSCO-0.49/0.49
SBSCO-0.48/0.48
SBSCO-0.47/0.47
SBSCO-0.46/0.46
SBSCO-0.45/0.45
SBSCO-0.49/0.5
SBSCO-0.48/0.5
SBSCO-0.47/0.5
SBSCO-0.46/0.5
SBSCO-0.45/0.5
20
40
60
80
2θ(deg.)

(a)

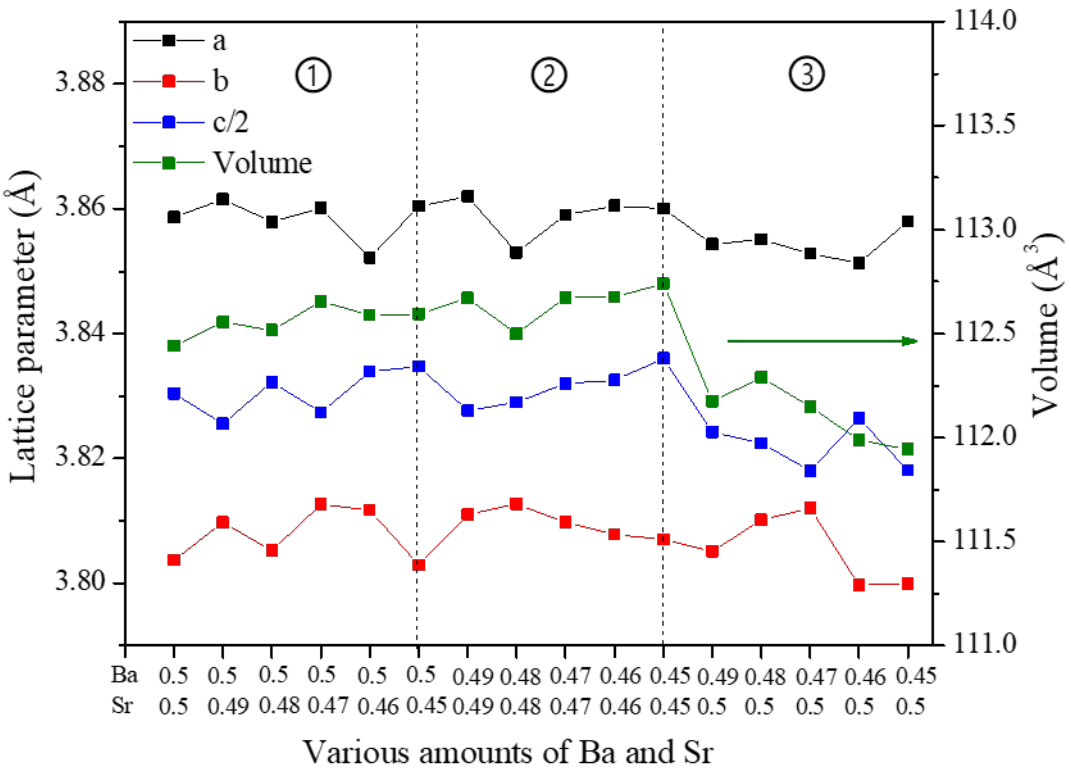

(b)

Figure 2. Results of (a) XRD and (b) lattice parameters of $SmBa_{0.5}Sr_{0.5-x}Co_2O_{5+d}$, $SmBa_{0.5-x}Sr_{0.5-x}Co_2O_{5+d}$ and $SmBa_{0.5-x}Sr_{0.5}Co_2O_{5+d}$ (x=0.01 ~ 0.05)

3. 2. Electrochemical characteristics of half-cells with non-stoichiometric cathode compositions

The ASR results of $SmBa_{0.5}Sr_{0.5-x}Co_2O_{5+d}$, $SmBa_{0.5-x}Sr_{0.5}Co_2O_{5+d}$ and $SmBa_{0.5-x}Sr_{0.5-x}Co_2O_{5+d}$ were summarized in Figure 3. (a). SBSCO-0.45/0.45 having the largest unit cell volume in section 3.1 showed ASRs of 1.020, 0.647, 0.428 and 0.320 Ωcm^2 at 650, 700, 750 and 800 ºC, which were the highest values compared to other compositions. However, the ASRs of SBSCO-0.45/0.5 with the smallest unit cell volume were 0.102, 0.058, 0.038 and 0.028 Ωcm^2 at the same temperature measured (650, 700, 750 and 800 ºC), which were

excellent values compared to other compositions. In particular, SBSCO-0.45/0.5 showed a lower value (0.102 Ωcm^2) at 650 ºC than 0.15 Ωcm^2, which is the maximum ASR required for IT-SOFC cathode [28]. SBSCO-0.45/0.5 showed a very low ASR value at 700 ºC compared to the ASR value of $SmBa_{0.5}Sr_{0.5}Co_2O_{5+d}$ (SBSCO-0.5/0.5), but also to cathode materials suggested in recent research like $PrBaCo_2O_{5+d}$ (0.233 Ωcm^2), $SmBaCo_2O_{5+d}$ (0.131 Ωcm^2), $PrBaCuCoO_{5+d}$ (0.047 Ωcm^2) and $SmBa_{0.8}Ca_{0.2}Co_2O_{5+d}$ (0.26 Ωcm^2) [17, 21, 29-31].

SBSCO-0.45/0.5 has the lowest TEC due to its small unit cell volume compared to other compositions. Part of the excellent ASR performance of SBSCO-0.45/0.5 can be attributed to its chemical stability in combination with the electrolyte material CGO91 because of its low TEC [32]. Also, the excellent ASR of SBSCO-0.45/0.5 can be explained by the result of XPS analysis. The O_{1s} spectra originated from different Ba and Sr substitution amounts were summarized in Figure 3. (b) and Table S2. The high binding energy (HBE) located at the ranges of 530.90 – 531.40 eV of the O_{1s} spectra of SBSCO-0.45/0.5, SBSCO-0.5/0.48, SBSCO-0.45/0.45 and SBSCO-0.46/0.46 is related to hydroxyls species (OH^-) and the surface adsorption of oxygen molecules [33-36]. The values of HBE area % of SBSCO-0.45/0.5, SBSCO-0.5/0.48, SBSCO-0.45/0.45 and SBSCO-0.46/0.46 were 48.99, 45.45, 42.85 and 45.26 %, with SBSCO-0.45/0.5 displaying the highest area %. Therefore, the ASR of SBSCO-0.45/0.5 was excellent because the HBE area % of the O_{1s} spectrum related to the adsorption of oxygen molecules.

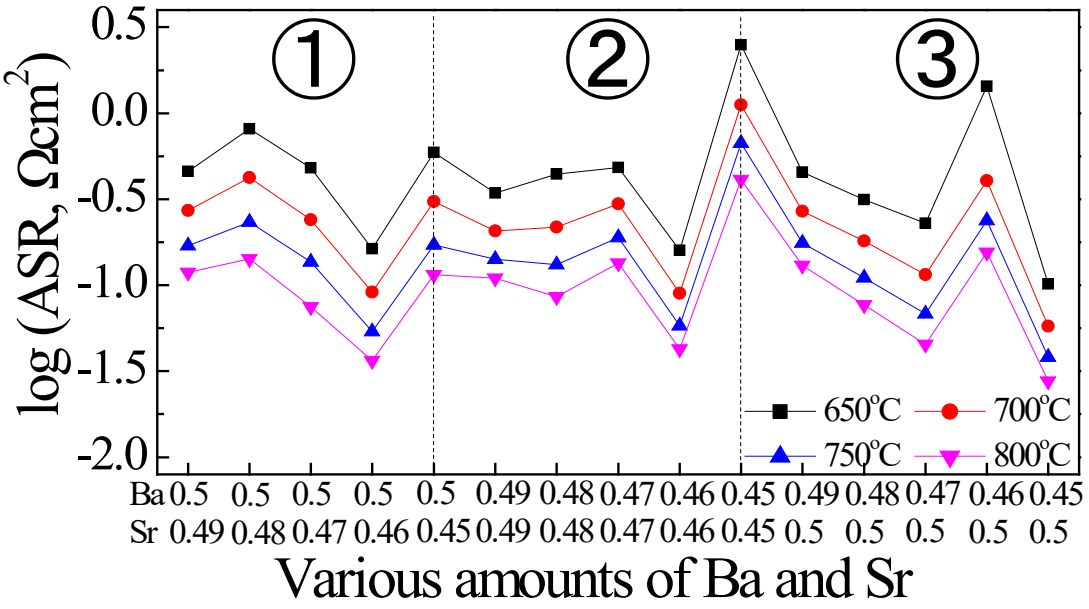
log (ASR, Ωcm^2)
0.5
0.0
-0.5
-1.0
-1.5
-2.0
①
②
③
650°C
700°C
750°C
800°C
Ba 0.5 0.5 0.5 0.5 0.5 0.49 0.48 0.47 0.46 0.45 0.49 0.48 0.47 0.46 0.45
Sr 0.49 0.48 0.47 0.46 0.45 0.49 0.48 0.47 0.46 0.45 0.5 0.5 0.5 0.5 0.5
Various amounts of Ba and Sr

(a)

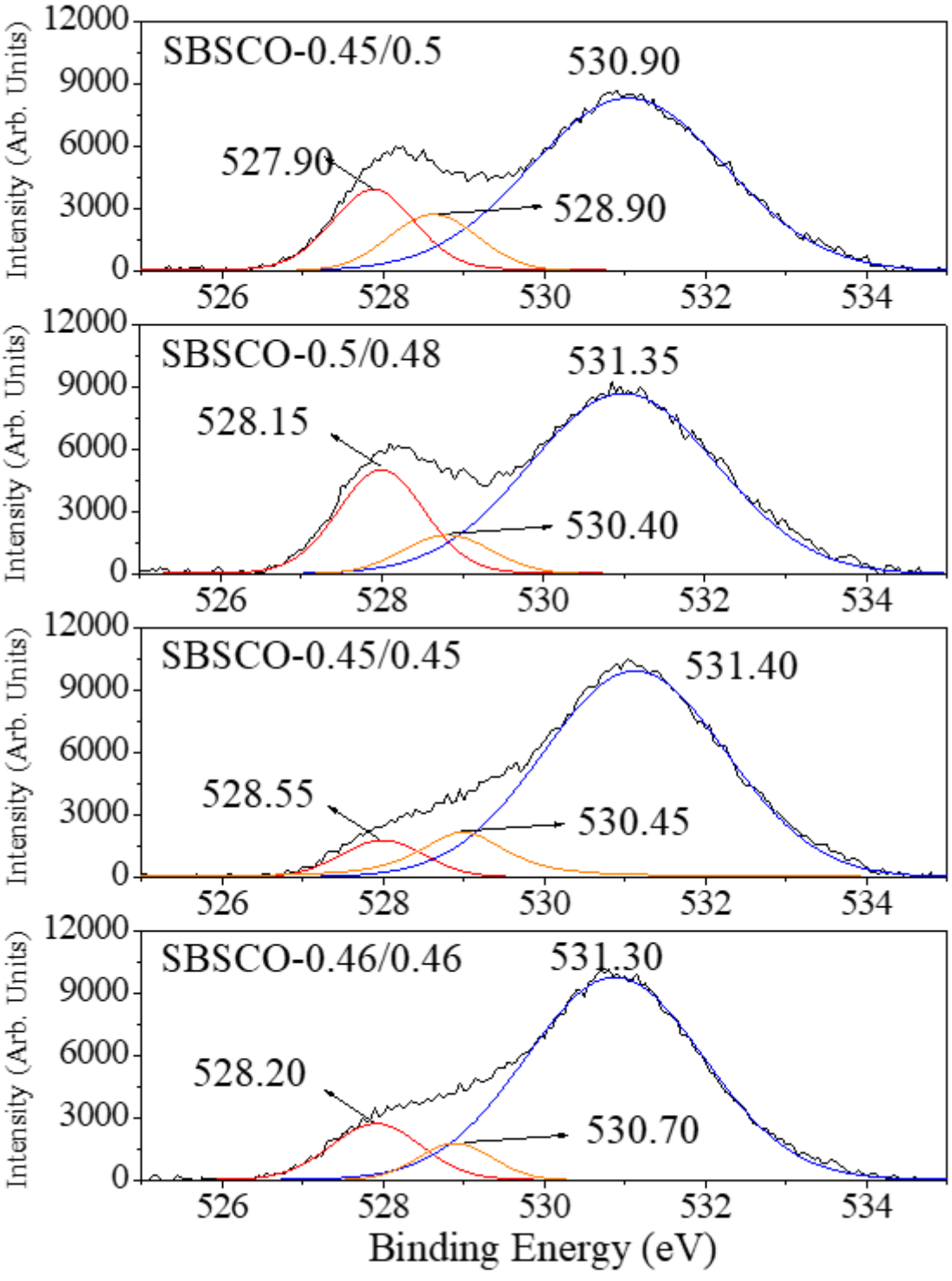

(b)

Figure 3. (a) The results of ASR of $SmBa_{0.5}Sr_{0.5-x}Co_2O_{5+d}$, $SmBa_{0.5-x}Sr_{0.5}Co_2O_{5+d}$, and $SmBa_{0.5-x}Sr_{0.5-x}Co_2O_{5+d}$ (x=0.01 ~ 0.05) at 650 ~ 800 ºC. (b) The results of oxygen spectra of SBSCO-

0.45/0.5, SBSCO-0.5/0.48, SBSCO-0.45/0.45 and SBSCO-0.46/0.46

Figure S1. (a) and (b) shows that R_1 (resistance of high frequency range, $10^2 \sim 10^3$ Hz) higher than R_2 (resistance of low frequency range, $10^{-1} \sim 10$ Hz) in the whole temperature range of 650 ~ 900 ºC for the cathode material SBSCO-0.45/0.5 [37, 38]. The conclusion from these results is that the rate determining step (RDS) of SBSCO-0.45/0.5 in the temperature range corresponding to IT-SOFCs was the ion conduction at the interface between electrode and electrolyte.

Figure S1. (c) and (d) shows the Nyquist plots of a single-cell with a composite cathode comprised of SBSCO-0.45/0.5 and CGO91. The ASR values of the composite cathode were 0.018, 0.017, 0.016 and 0.016 Ωcm^2 at 700, 750, 800 and 850 ºC, lower than single-phase SBSCO-0.45/0.5. The reason for the decreased ASR of the composite cathodes is not only their extended triple phase boundary (TPB) between the electrode and the electrolyte and the enhanced oxygen ion conduction but also the minimized TEC difference between the cathode and the electrolyte by mixing CGO91 with the cathode material [39, 40].

Figure S2 summarizes the results of a HT-XRD analysis of SBSCO-0.45/0.5, the composition which has the lowest ASR amongst all compositions. SBSCO-0.45/0.5 maintains XRD peaks that can be identified as layered perovskite even at a high temperature [22]. Peak splitting at 23, 47 and 59 º was observed in all temperatures measured, and no secondary phase was found [23, 24]. This indicates that the orthorhombic structure forming the basic frame of SBSCO-0.45/0.5 was maintained at all temperatures ranges and is structurally stable even at high temperature.

3. 3. Electrical conductivities of dense microstructure samples

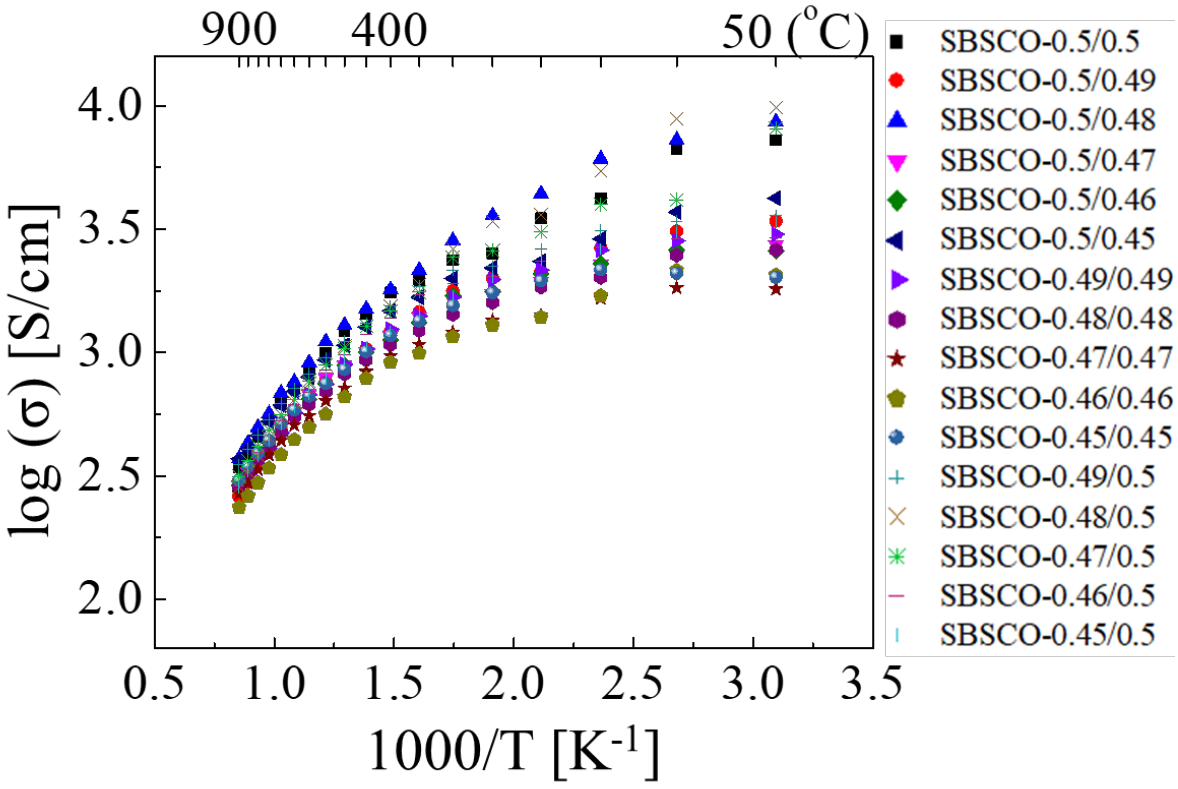

Figure 4. Electrical conductivities with applied current of 0.1 A at 50 ~ 900 ºC.

Electrical conductivities of dense $SmBa_{0.5}Sr_{0.5-x}Co_2O_{5+d}$, $SmBa_{0.5-x}Sr_{0.5}Co_2O_{5+d}$ and $SmBa_{0.5-x}Sr_{0.5-x}Co_2O_{5+d}$ in the temperature range between 50 and 900 ºC were summarized in Figure 4. These oxide systems showed metallic electrical conductivity behavior in which the electrical conductivity decreases with increasing temperature [41]. The decreased electrical conductivity value with increasing temperature is caused by the saturation of Co^{4+} and then reduction of Co^{4+} to Co^{3+} as well as the oxygen vacancy that occurs as a function of the temperature inside the lattice increases [41].

In particular, all compositions in Figure 4 showed a rapid decrease in electrical conductivity values in the vicinity of 300 ºC, which can be explained using Figures 5. (a) ~ (c). Figure 5. (a)

is the result of summarizing the TEC of SBSCO-0.5/0.5, which is a stoichiometric composition representing all compositions, and the TEC values were 17.1 x 10^{-6}, 20.8 x 10^{-6}, 21.5 x 10^{-6}, 22.3 x 10^{-6} and 22.8 x 10^{-6} K^{-1} at 300, 600, 700, 800 and 900 ºC, respectively. With an increase in temperature the number of oxygen vacancies in the lattice increases. Missing oxide anions in the lattice mean that the repulsion force between two cations, which are now neighbors, can't be mitigated by the negative charge of an anion between them. In addition, as the temperature increases, an increasing fraction of the B-site cations is reduced to Co^{3+}, which has a larger ionic radius than Co^{4+}, leading to further expansion of the lattice. Therefore, the unmitigated repulsion between the cations and the increase of the number of Co^{3+} ions both cause the lattice to enlarge, showing in an increase of lattice parameters and TEC [32].

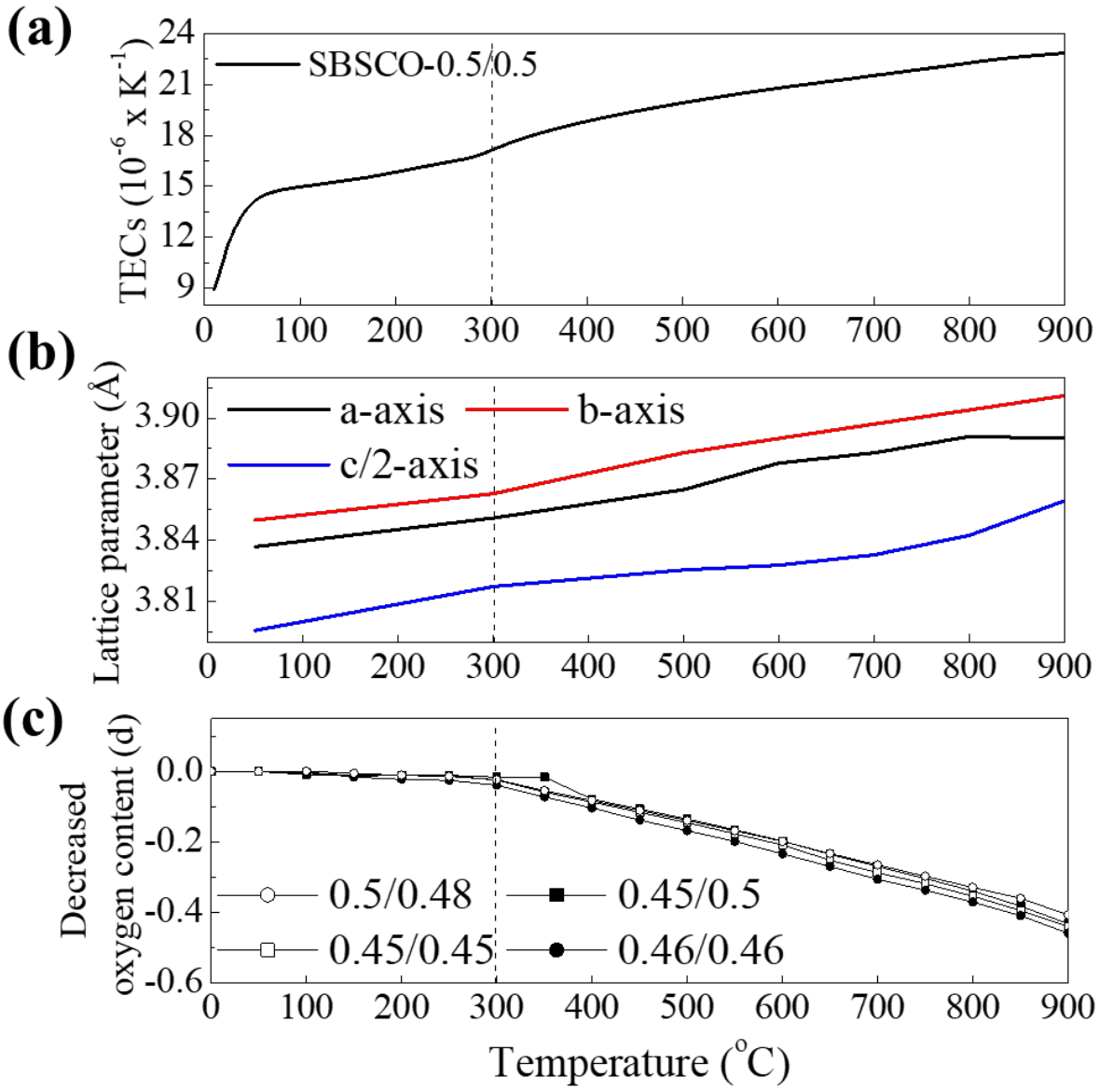

Figure 5. (a) TEC result of SBSCO-0.5/0.5. (b) HT-XRD result of SBSCO-0.45/0.5. (c) TGA results of SBSCO-0.5/0.48, SBSCO-0.45/0.5, SBSCO-0.45/0.45 and SBSCO-0.46/0.46.

Figure 5. (b) and Table S3 show the HT-XRD analysis results of SBSCO-0.45/0.5 at different temperatures as a diagram and in table form. SBSCO-0.45/0.5 is the composition with the lowest ASR. The a, b and c-axis lattice parameters of SBSCO-0.45/0.5 were in the ranges of

3.837–3.890, 3.850–3.911 and 7.592–7.719 Å. Especially, the a and c-axis slopes change as they rapidly increase to 3.837–3.851 Å and 7.592–7.635 Å, respectively, in the temperature range of 50 to 300 ºC. This is due to the rapid increase in oxygen vacancy in these temperature ranges [42].

Figure 5. (c) shows the reduction of oxygen in the lattice of SBSCO-0.5/0.48, SBSCO-0.45/0.5, SBSCO-0.45/0.45 and SBSCO-0.46/0.46 in % of the total lattice oxygen, calculated from TGA results. SBSCO-0.5/0.48, SBSCO-0.45/0.5, SBSCO-0.45/0.45 and SBSCO-0.46/0.46 showed a rapid decrease of oxygen contents from about 300 ºC because of the generation of oxygen vacancies in the lattice. A large amount of oxygen vacancies is generated at about 300 ºC in the lattice of SBSCO, both in the stoichiometric composition and in the non-stoichiometric composition [42]. This phenomenon can be seen in the change of the slope in Figures 5. (a) ~ (c), and it also can be seen that the electrical conductivity decreases rapidly at 300 ºC in Figure 4.

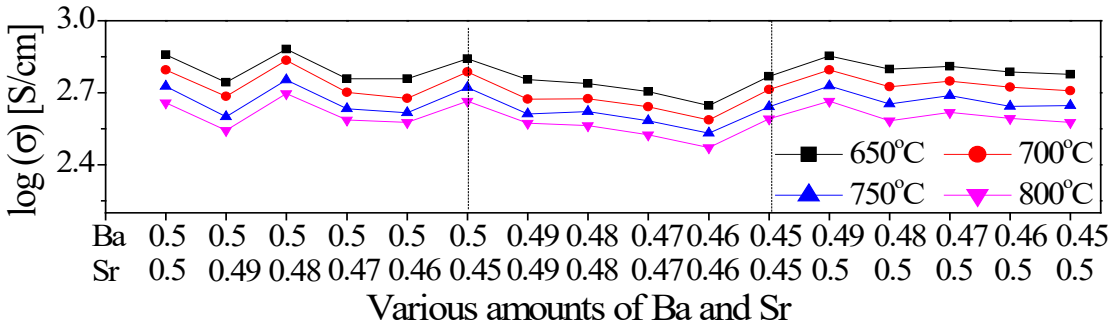

Figure 6. Electrical conductivities of dense cathodes at 650 ~ 800 ºC

Figure 6 shows the electrical conductivities at 650 ~ 800 ºC with an applied current of 0.1 A. The electrical conductivities of SBSCO-0.5/0.48 were 1096.98 and 389.05 S/cm at 50 and 700 ºC, showing the highest electrical conductivity when compared to other compositions. SBSCO-0.46/0.46 has an electrical conductivity of 639.57 and 250.72 S/cm under the same applied current and temperature conditions, and it shows the lowest electrical conductivity when compared with the results of other compositions.

When these characteristics are analyzed using the TGA analysis results in Figure 5. (c) and Table S4, it can be explained in terms of oxygen contents (or oxygen vacancy). SBSCO-0.5/0.48 showed the lowest oxygen content reduction (0.41), and thus resulted in highest electrical conductivity because oxygen vacancy was generated the least. However, SBSCO-0.46/0.46 showed the lowest electrical conductivity value because of the highest oxygen content reduction (0.46) indicating the creation of the largest amount of oxygen vacancies in this composition.

In addition, the electrical conductivities of SBSCO-0.5/0.48 can be specified and explained using XPS analysis. When analyzing the Co_{2p} spectra results of SBSCO-0.45/0.5. SBSCO-

0.5/0.48, SBSCO-0.45/0.45 and SBSCO-0.46/0.46 are presented in Figure 7 and Table S5. The first broad satellite peaks originate from the mixed Co charge state of Co^{2+} and Co^{4+} in the vicinity of 787.75 – 789.50 eV, and the second broad satellite peaks are ascribed to the mixed Co charge state of Co^{3+} and Co^{4+} in the vicinity of 803.60–804.50 eV [33, 35]. The values of area % of first satellite peaks of SBSCO-0.45/0.5. SBSCO-0.5/0.48, SBSCO-0.45/0.45 and SBSCO-0.46/0.46 were 3.29, 3.14, 3.43 and 3.78 %. It can be observed that SBSCO-0.46/0.46 has the lowest electrical conductivity because of the highest area % of the first satellite peak compared to other compositions. The values of the area % of the second satellite peaks of SBSCO-0.45/0.5. SBSCO-0.5/0.48, SBSCO-0.45/0.45 and SBSCO-0.46/0.46 were confirmed to be 11.59, 12.62, 11.07 and 11.08 %, respectively. When these results are connected with their electrical conductivity, SBSCO-0.5/0.48, which shows the largest value of Area% of the spectrum where Co^{3+} and Co^{4+} coexist, has the highest electrical conductivity at room temperature.

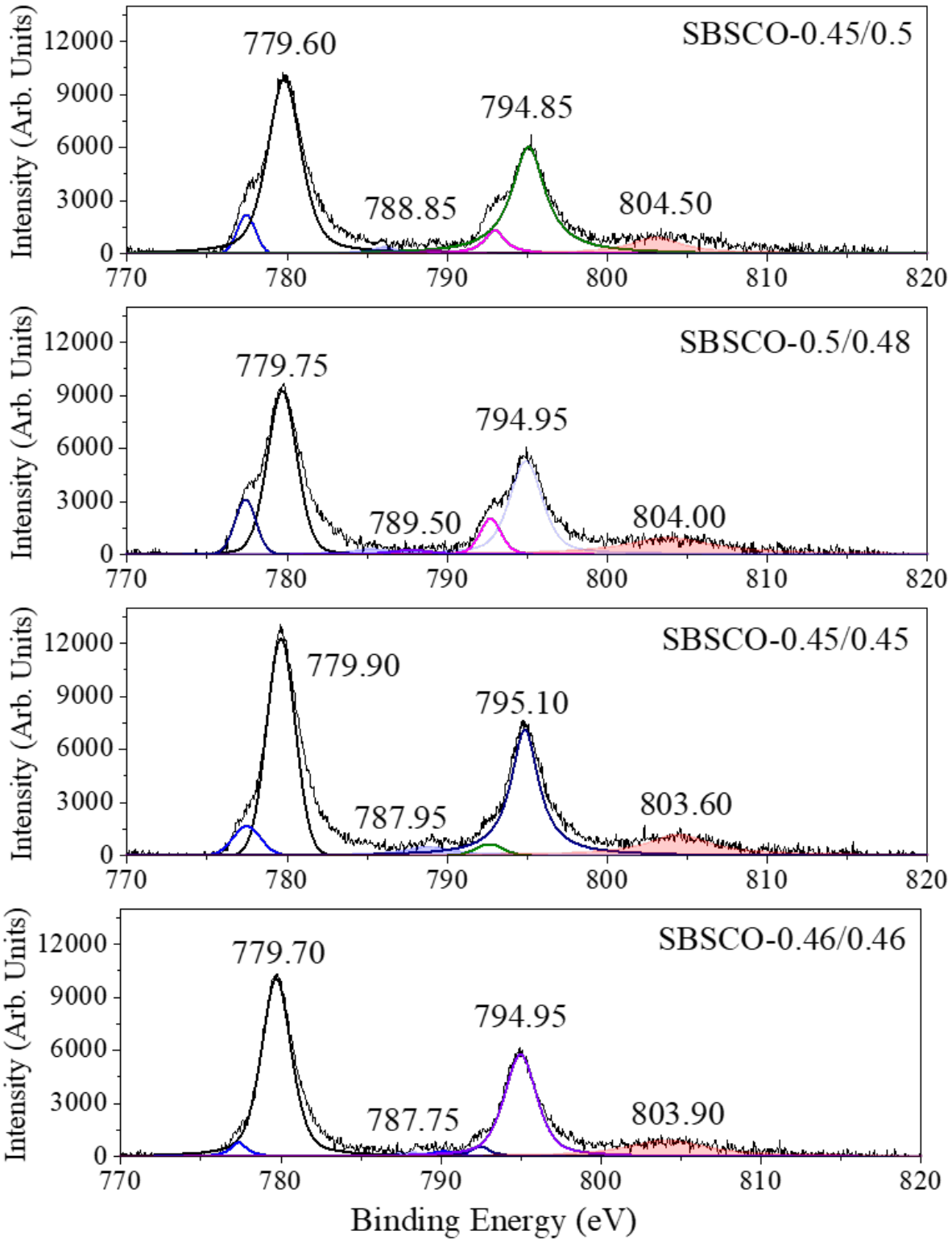

Figure 7. Cobalt spectra of SBSCO-0.45/0.5, SBSCO-0.5/0.48, SBSCO-0.45/0.45, and

SBSCO-0.46/0.46

Electrical conductivities at the experimental condition of heating cycle in air (■) and cooling cycle in air (□) were summarized in Figures 8. (a) and (b). SBSCO-0.5/0.48 and SBSCO-0.45/0.5 showed typical metallic behavior in which the electrical conductivity decreases with increasing temperature at the experimental condition of heating cycles and cooling cycles in air. There were no marked differences between the values in the high temperature range of heating and cooling cycles in air. For example, electrical conductivities of SBSCO-0.5/0.48 at heating cycle (■) and cooling cycle (□) in air were 1146.2 and 927.0 S/cm at 100 ºC and 389.1 and 346.1 S/cm at 700 ºC. The values of SBSCO-0.45/0.5 at heating cycle (■) and cooling cycle (□) in air were 965.2 and 873.7 S/cm at 100 ºC and 344.9 and 350.6 S/cm at 700 ºC in the same experimental conditions. That shows that since the dense cathode maintains thermal stability during the thermal cycle in air condition, there was no significant difference in the electrical conductivity behavior and the electrical conductivity values between the heating cycle and cooling cycle in air [43].

The heating cycle in N_2 (red scatter plots ■) can be compared with the heating cycle in Air (black scatter plots ■). From Figures 8. (a) and (b), the electrical conductivities of SBSCO-0.5/0.48 and SBSCO-0.45/0.5 measured in the heating cycle in N_2 were lower than the electrical conductivities measured in the heating cycle in air. For example, the electrical conductivities of SBSCO-0.5/0.48 were 887.6 and 517.2 S/cm in the heating cycle under air and N_2 condition at 300 ºC, and those of SBSCO-0.45/0.5 were 745.2 and 528.5 S/cm under the same experimental condition. This is because the electrical conductivities of SBSCO-0.5/0.48 and SBSCO-0.45/0.5 follow a typical p-type conductor behavior [44]. In addition, as

can be seen in Figure 8. (a) and (b), SBSCO-0.5/0.48 and SBSCO-0.45/0.5 showed metallic conductor behavior in the heating cycle in air and in the cooling cycle in air, but changed to semiconductor behavior in the cooling cycle in N_2. It can be seen that the conductivity behavior is changed because thermal stability cannot be maintained during high operating temperature and low partial pressure of oxygen [45, 46]

Figures 8. (c) and (d) show the electrical conductivities of dense SBSCO-0.5/0.48 and SBSCO-0.45/0.5 samples by applying various currents of 0.1, 0.5 and 1 A. The values of SBSCO-0.5/0.48 in Figure 8. (c) were 760.2, 466.4 and 437.1 S/cm in heating cycle in air at 650 ºC with applied currents of 0.1 (■), 0.5 (●) and 1 (▲) A, respectively, and the values of SBSCO-0.45/0.5 in Figure 8. (d) were 596.9, 401.7 and 381.5 S/cm at the same measurement conditions. As a result, the electrical conductivity values of dense cathodes with an applied current of 0.1 A were higher than the conductivity values with applied higher currents because charge carrier movement was activated when a lower current was applied [47, 48]. At lower currents, fewer of these charge carriers must move through the same crystal lattice, and the movement of charge carriers in the lattice is activated and the electrical conductivity increases than at higher currents [47, 48].

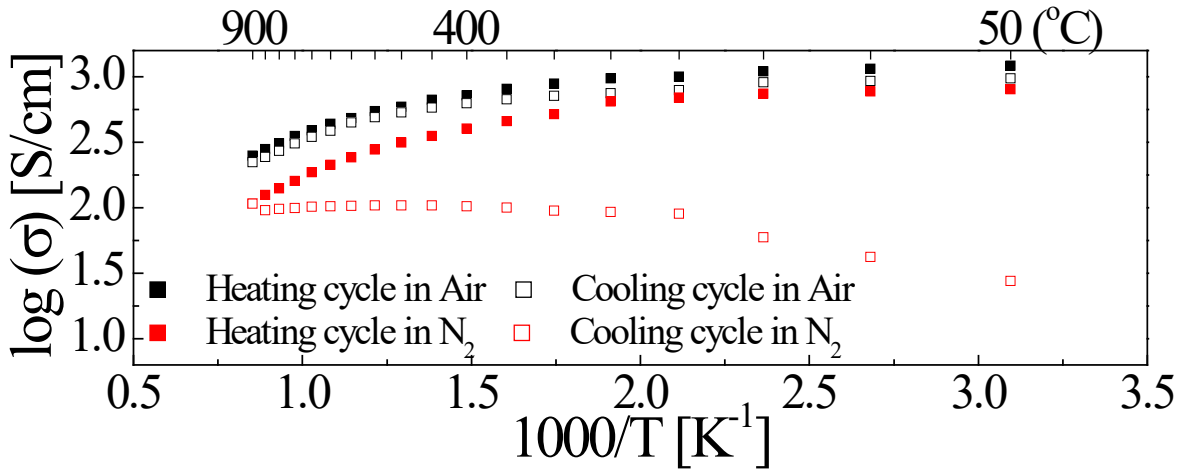
900
400
50 (°C)
log (σ) [S/cm]
3.0
2.5
2.0
1.5
1.0
Heating cycle in Air
Heating cycle in N2
Cooling cycle in Air
Cooling cycle in N2
0.5
1.0
1.5
2.0
2.5
3.0
3.5
1000/T [K-1]

(a)

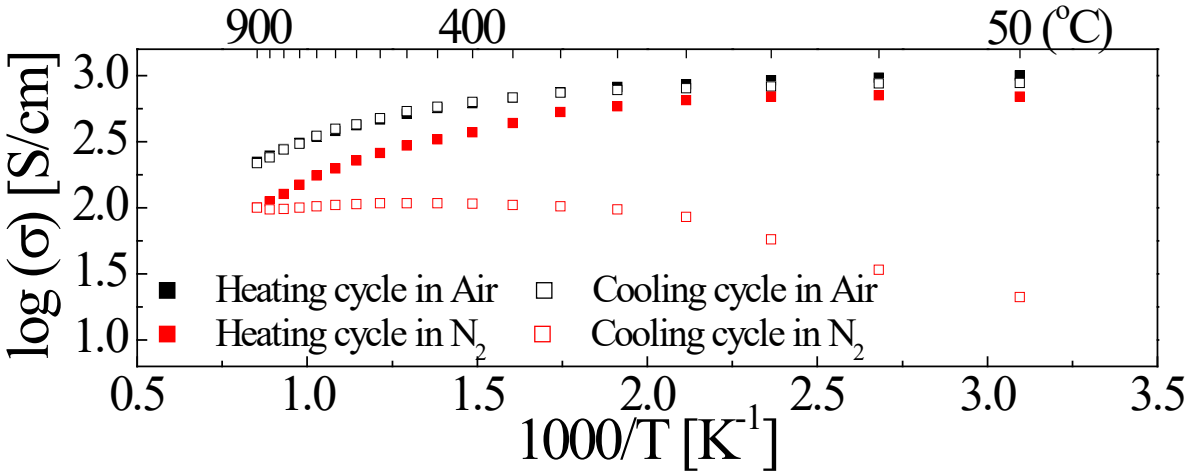
900
400
50 (°C)
log (σ) [S/cm]
3.0
2.5
2.0
1.5
1.0
Heating cycle in Air
Heating cycle in N2
Cooling cycle in Air
Cooling cycle in N2
0.5
1.0
1.5
2.0
2.5
3.0
3.5
1000/T [K-1]

(b)

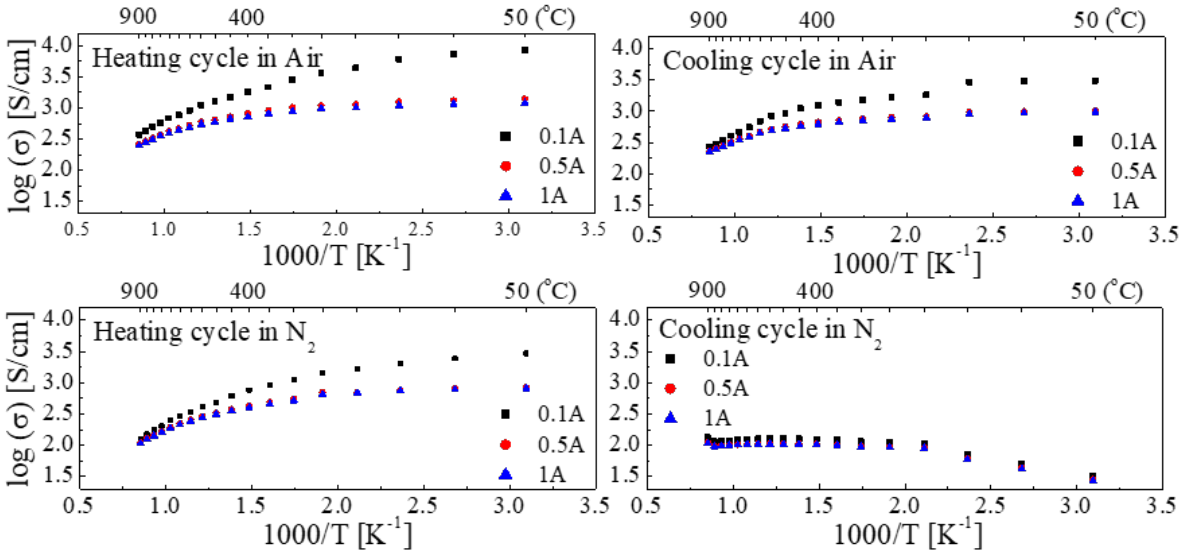

(c)

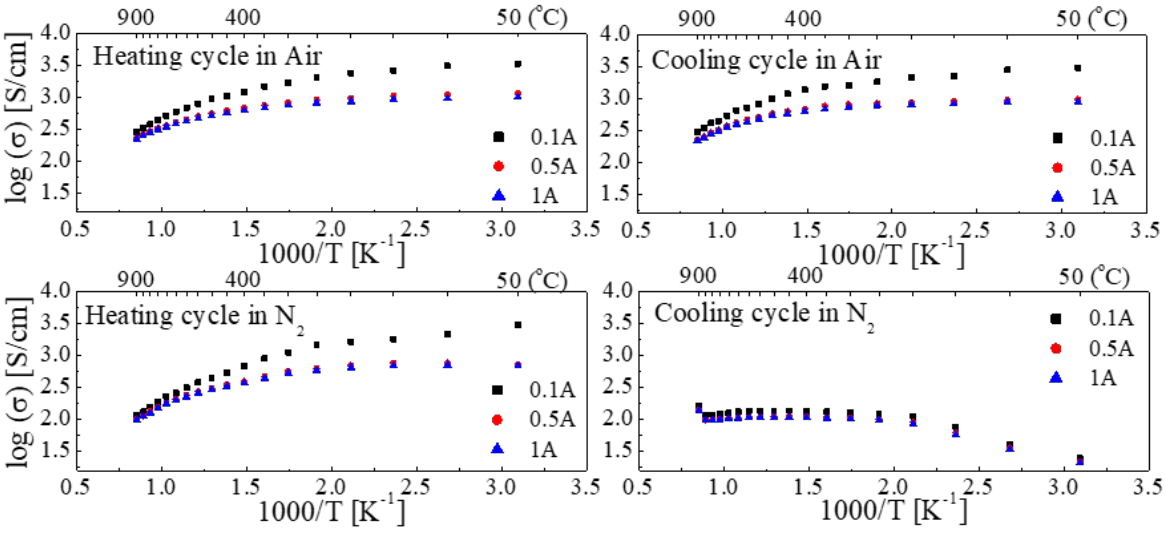

(d)

Figure 8. The electrical conductivities under various measurement conditions of dense (a) SBSCO-0.5/0.48 and (b) SBSCO-0.45/0.5. The electrical conductivities according to applied currents (0.1, 0.5 and 1 A) of dense (c) SBSCO-0.5/0.48 and (d) SBSCO-0.45/0.5

3. 4. Electrical conductivities of porous microstructure samples

The electrical conductivities of SBSCO-0.45/0.5 and SBSCO-0.5/0.48 having porous microstructure were summarized in Figure 9. It can be seen that the electrical conductivity of the porous cathodes SBSCO-0.45/0.5G, SBSCO-0.45/0.5Y, SBSCO-0.5/0.48G and SBSCO-0.5/0.48Y in Figure 9. (a) ~ (d) show lower values compared to the conductivity of the dense cathodes summarized in Figures 8. (a) and (b). For example, the electrical conductivities of H-0.45/0.5G were 24.8 and 83.0 S/cm at 100 and 700 ^{o}C in the heating cycle in air as shown in Figure 9. (a), and electrical conductivities of H-0.5/0.48G were 36.5 and 94.6 S/cm as shown in Figure 9. (c) at the same temperatures and conditions. This can be understood regarding the fact that the holes, which are the main charge carriers in a p-type conductor, are particularly restricted in movement in a porous structure, resulting in longer conductivity pathways and reduced conductivity values compared to the dense cathode [19, 49].

However, all porous cathodes exceeded a value of 100 S/cm, a value of conductivity required for IT-SOFC cathodes above 800 ^{o}C, regardless of the composition and the type of electrolyte materials [50, 51]. In addition, the dense cathodes in Figures 8. (a) and (b) showed metallic behavior with conductivity decreasing with increasing temperature, but the porous cathodes in Figures 9. (a) ~ d showed semiconductor behavior with electrical conductivity increasing with increasing temperature [52]. In other words, it can be seen that both the electrical conductivity behavior and the conductivity values change as the microstructure changes from the dense microstructure to porous microstructure as shown in Figures 9. (a) ~ (d) even though the same cathode compositions were used [19].

Comparing the electrical conductivities in air atmosphere (■) and N_2 atmosphere (■) in Figures 9. (a) ~ (d), conductivities of all porous cathodes were higher in air atmosphere than in

N_2 atmosphere at all measurement temperatures. The electrical conductivities of H-0.45/0.5G, which has the highest electrical conductivity of all porous cathodes, were 110.0 and 171.1 S/cm in heating cycle in air, and 96.3 and 131.1 S/cm in heating cycle in N_2 at 650 and 900 ºC as shown in Figure 9. (a). The electrical conductivities of H-0.5/0.48G in Figure 9. (c) were 83.51 and 120.8 S/cm at 650 and 900 ºC in the heating cycle in air, and 71.3 and 91.2 S/cm at 650 and 900 ºC in the heating cycle in N_2.

In summary, it can be seen that a higher oxygen partial pressure results in a higher electrical conductivity value in cathodes of all different compositions studied and both for samples with dense microstructure and for samples with porous microstructure. The reason for this is that samples measured under high oxygen partial pressure have an increased concentration of holes, which are conduction carriers in a p-type conductor, no matter if the sample is dense or porous [19, 49]. The porous cathodes in Figures 9. (a) ~ (d) did not show any change in electrical conductivity behavior along with the decrease in oxygen partial pressure. That shows that a change in the oxygen partial pressure does not affect the electrical conductivity behavior of porous cathodes [19].

Most of the porous cathodes in Figures 9. (a) ~ (d) show higher electrical conductivity during the cooling cycle (□) than during the heating cycle (■). For example, the conductivities of H-0.45/0.5G at same measurement conditions in Figure 9. (a) were 120.2 and 155.1 S/cm during the heating cycle and cooling cycle. This can be attributed to the fact that sufficient thermal activation has already been applied to the porous cathode in the case of the cooling cycle starting at high temperature rather than during the heating cycle starting at low temperature. As a result, the hole mobility in the cathode during the cooling cycle is greater than the hole mobility during the heating cycle [19, 49].

In addition to these characteristics, a rapid decrease of electrical conductivity at about 700 ºC in the cooling cycle in air and N_2 was observed in all samples in Figures 9. (a) ~ (d). This is related to the phenomenon that the oxygen content increases while the temperature decreases. As reported by Genouel et al and Kim et al, it can be explained that the oxygen contents decreased in the heating cycle increase in the cooling cycle [53, 54]. Since oxygen contents have a characteristic that changes reversibly according to temperature and oxygen partial pressure, oxygen vacancies decrease according to temperature decrease in the temperature range of 900 ~ 700 ºC during the cooling cycle. However, below 700 ºC, the concentration of Co^{2+} and Co^{4+} increases, resulting in a rapid decrease in electrical conductivity [53, 54].

The electrical conductivities of H-0.45/0.5G at different applied currents were summarized in Figure 9. (e). It was already confirmed through Figures 8. (c) and (d) that the Co substituted cathodes forming a dense structure had higher electrical conductivity as a lower current was applied. However, the porous H-0.45/0.5G cathode showed 96.8, 96.4, 95.8 and 94.6 S/cm with applied currents of 0.05, 0.075, 0.1 and 0.3 A under heating cycle in air at 750 ºC. Since the main limitation of the movement of the charge carriers is the pores, the porous cathode shows almost the same conductivity values regardless of the applied currents because the current density does not affect the electrical conductivity [55-57].

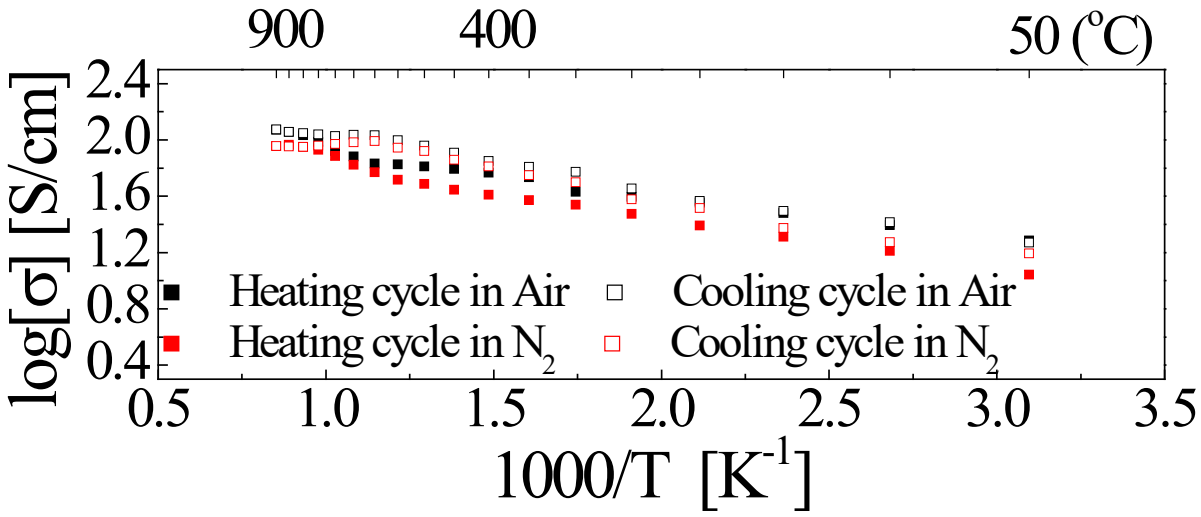
900
400
50 (°C)
log[σ] [S/cm]
2.4
2.0
1.6
1.2
0.8
0.4
Heating cycle in Air
Heating cycle in N2
Cooling cycle in Air
Cooling cycle in N2
0.5
1.0
1.5
2.0
2.5
3.0
3.5
1000/T [K-1]

(a)

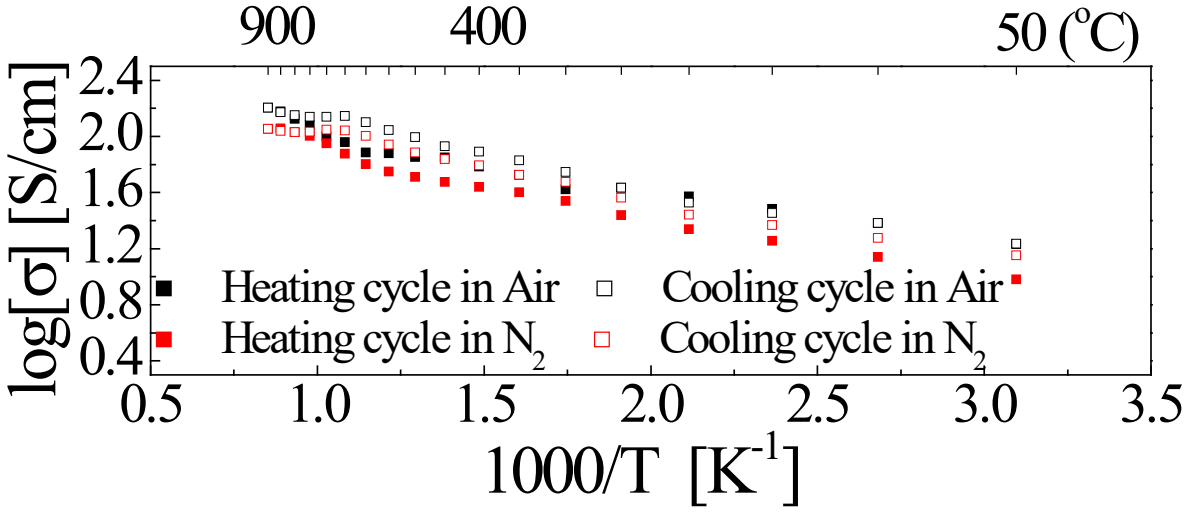
900
400
50 (°C)
log[σ] [S/cm]
2.4
2.0
1.6
1.2
0.8
0.4
Heating cycle in Air
Heating cycle in N2
Cooling cycle in Air
Cooling cycle in N2
0.5
1.0
1.5
2.0
2.5
3.0
3.5
1000/T [K-1]

(b)

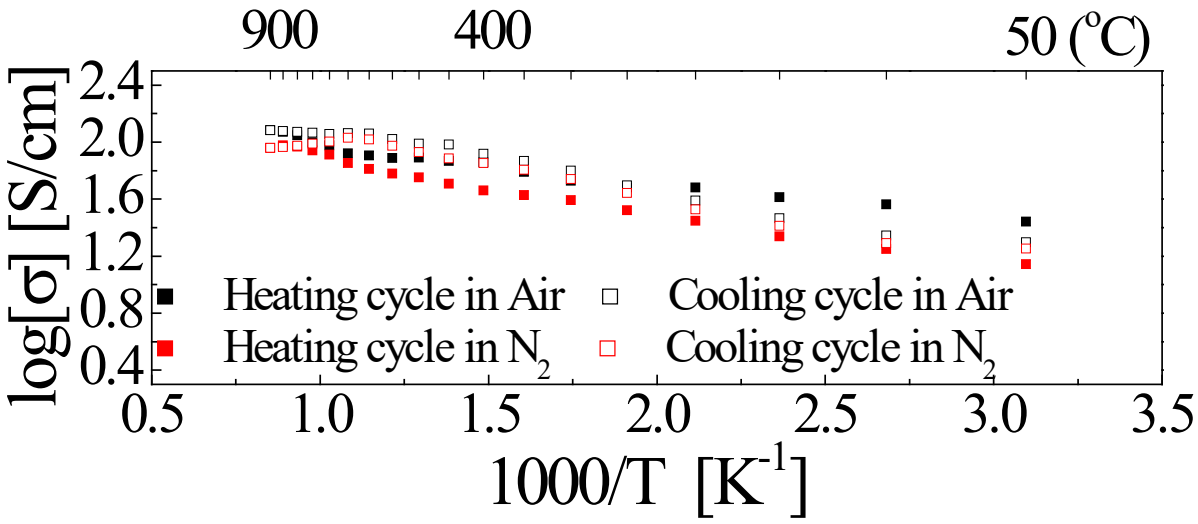
900
400
50 (°C)
log[σ] [S/cm]
2.4
2.0
1.6
1.2
0.8
0.4
Heating cycle in Air
Heating cycle in N2
Cooling cycle in Air
Cooling cycle in N2
0.5
1.0
1.5
2.0
2.5
3.0
3.5
1000/T [K-1]

(c)

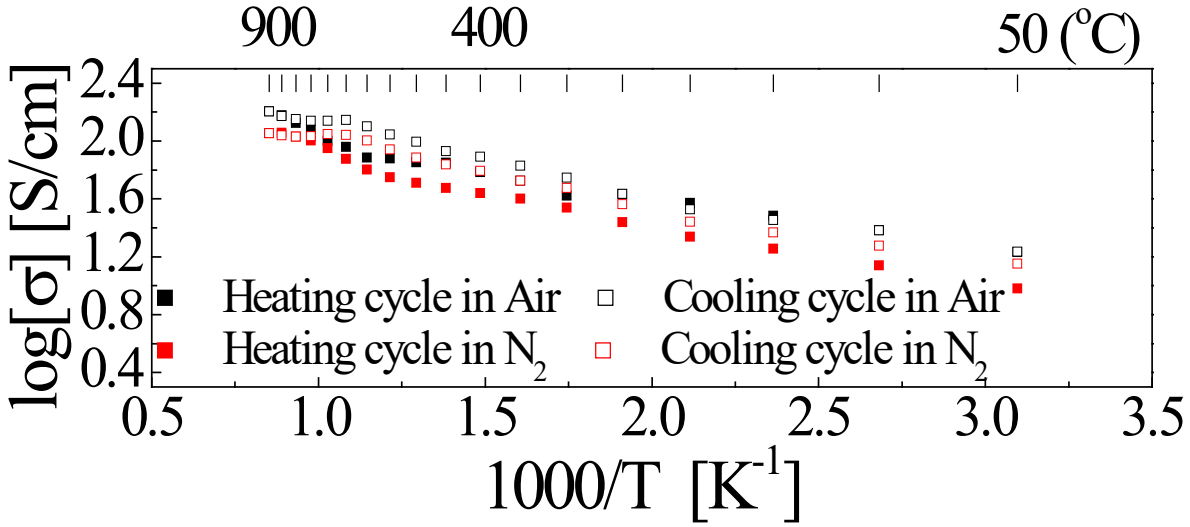
900
400
50 (°C)
log[σ] [S/cm]
2.4
2.0
1.6
1.2
0.8
0.4
Heating cycle in Air
Heating cycle in N2
Cooling cycle in Air
Cooling cycle in N2
0.5
1.0
1.5
2.0
2.5
3.0
3.5
1000/T [K-1]

(d)

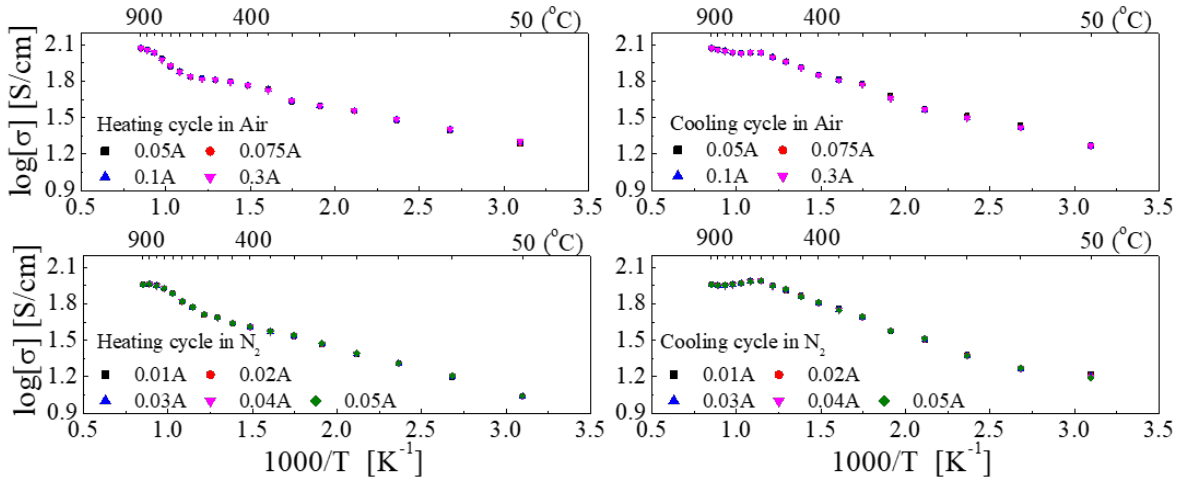

(e)

Figure 9. The results of electrical conductivities of (a) H-0.45/0.5 G, (b) H-0.45/0.5Y, (c) H-0.5/0.48G and (d) H-0.5/0.48Y. The electrical conductivities of (e) H-0.45/0.5G according to applied currents

3. 5. Microstructural properties

The microstructures of the dense and of the porous cathode were summarized in Figures S3. As can be seen in Figure S3. (a) and (b), the porous cathode showed low inter-particle bonding characteristics and low density compared to the bar shaped dense cathode sample. Figure S3. (c) shows the Focused ion beam (FIB) results of the dense and the porous microstructural cathodes. From the results, it can be seen that the dense cathode has large contact areas, and the porous cathode has small and narrow contact areas. A dense cathode having high density such as SBSCO-0.5/0.5 has a large contact area between particles or grains, so an easy path for charge carriers to move to nearby particles is created. This microstructural characteristic results in the forming of continuous electrical paths inside the cathode, so the dense cathode exhibits

excellent electrical conductivity. However, a porous cathode with low density such as H-0.45/0.5G has relatively small and narrow contact areas between particles or grains in the cathode, so the movement of charge carriers inside the cathode is limited and a discontinuous electric path is formed, resulting in low electrical conductivity [19, 55-58].

3. 6. Single cell performance

The power density of a SBSCO-0.45/0.5 based single-cell and of a SBSCO-0.5/0.48 single-cell were measured and summarized in Figures 10. (a), (b) and Table S6 [59]. The SBSCO-0.45/0.5 single-cell showed maximum power densities of 0.5614 and 0.6616 W/cm^2 at 800 and 850 ºC as shown in Figure 10. (a), which is higher than the maximum power density required for IT-SOFCs of 0.5 W/cm^2 [60]. However, the maximum power densities of SBSCO-0.5/0.48 single-cell in Figure 10. (b) were 0.019 and 0.027 W/cm^2 at the same temperatures, showing lower power densities compared to SBSCO-0.45/0.5 single-cell. The reason that the power density of the SBSCO-0.45/0.5 single-cell is higher than that of the SBSCO-0.5/0.48 single-cell is because the polarization resistance (R_p) of SBSCO-0.45/0.5 cathode was lower than that of the cell with the SBSCO-0.5/0.48 cathode. SBSCO-0.5/0.48 shows high electrical conductivity, but lower power density than SBSCO-0.45/0.5, which shows relatively low ASR. Therefore, when measuring the power density of non-stoichiometric cathodes based on the two variables of ASR and electrical conductivity, it can be seen that a composition with a low ASR shows a higher power density [42, 61].

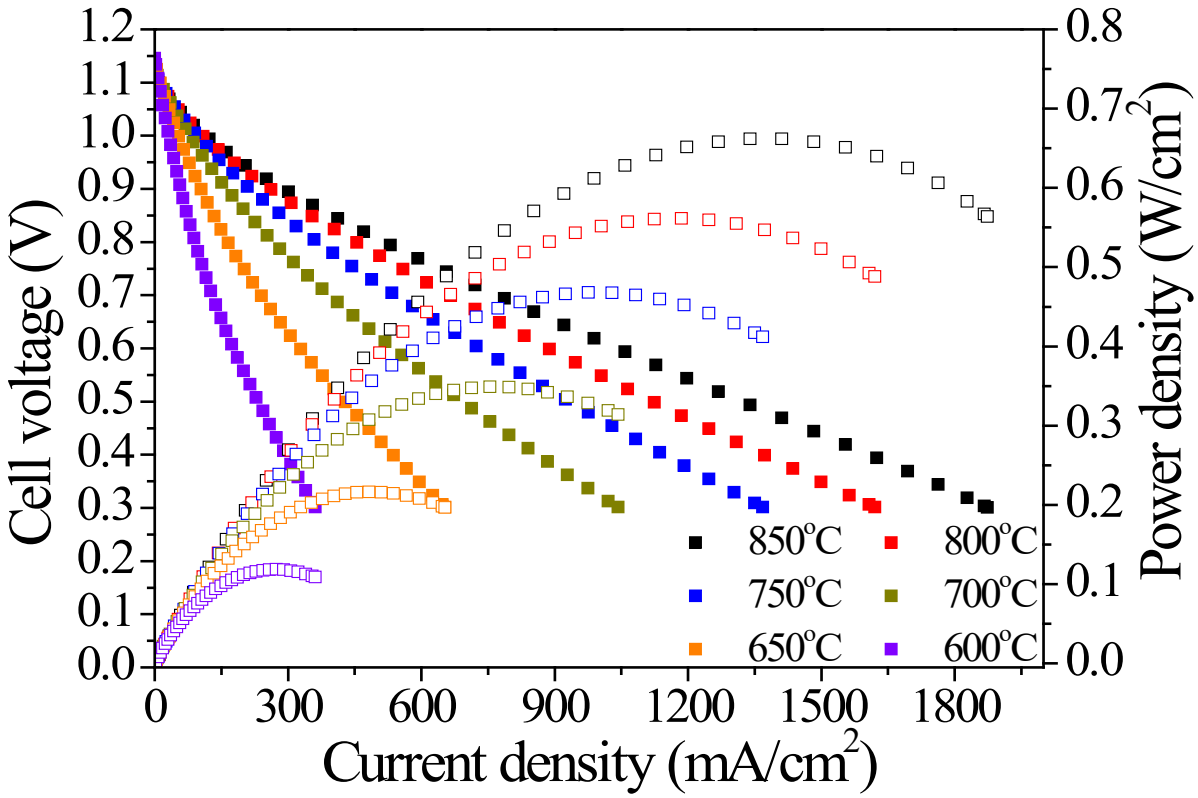
Cell voltage (V)
Power density (W/cm^2)
Current density (mA/cm^2)
850°C
800°C
750°C
700°C
650°C
600°C

(a)

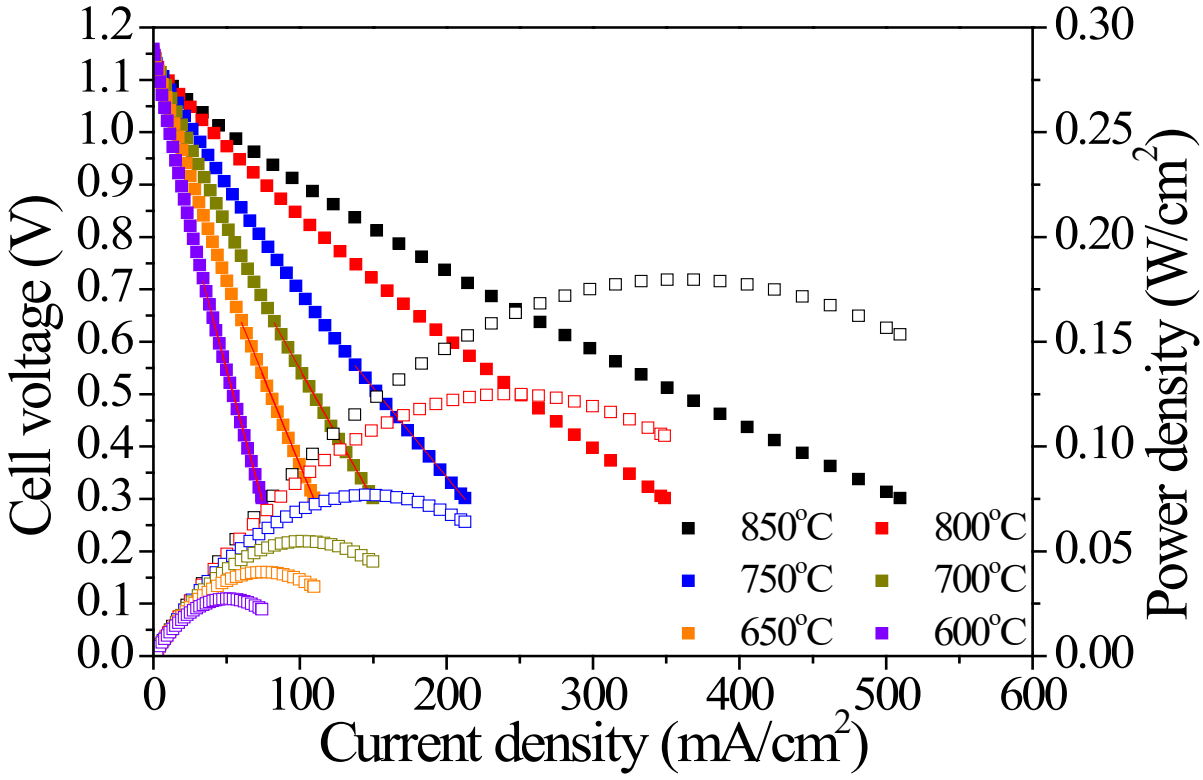

(b)

Figure 10. Power densities of (a) SBSCO-0.45/0.5 single-cell and (b) SBSCO-0.5/0.48 single-cell

4. Conclusion

In this study, the electrochemical properties of $SmBa_{0.5}Sr_{0.5-x}Co_2O_{5+d}$, $SmBa_{0.5-x}Sr_{0.5}Co_2O_{5+d}$ and $SmBa_{0.5-x}Sr_{0.5-x}Co_2O_{5+d}$ (x = 0.01 ~ 0.05) layered perovskite oxide systems with non-stoichiometric composition were studied with respect to the substitution amount of Ba and Sr. The lowest unit cell volume characteristic was observed in the SBSCO-0.45/0.5 composition, which can minimize the TEC difference between electrode and electrolyte. Accordingly, physical and chemical stability of a cell with the electrolyte may be maintained

as well as good resistance against thermal expansion. In addition, when analyzing ASR characteristics by linking them with XPS analysis results, SBSCO-0.45/0.5, which has the highest high binding energy area % of O_{1s} compared to other samples, shows the lowest ASR characteristics. The dense SBSCO-0.5/0.48 showed the highest electrical conductivity value, and it was confirmed that the decrease in oxygen contents was low and the area % of the second satellite peak of the Co_{2p} spectrum was high. The electrical conductivities of porous SBSCO-0.45/0.5 and SBSCO-0.5/0.48 were higher than 100 S/cm at 800 ^{o}C. As a result of the single-cell performance comparison between SBSCO-0.45/0.5 and SBSCO-0.5/0.48, the single-cell with the SBSCO-0.45/0.5 cathode showed a higher maximum power density. In other words, the single-cell with SBSCO-0.45/0.5 having low ASR showed excellent performance. Therefore, SBSCO-0.45/0.5 showed higher performance, better thermal stability and better chemical stability compared to other non-stoichiometric compositions, and it was confirmed that it could be used as an excellent cathode for IT-SOFCs.

Acknowledgments

This work was supported by the National Research Foundation of Korea (NRF) grant funded by the Ministry of Science and ICT (MSIT) of the Korean government (No. 2019R1A2C1087534) and by the Commercialization Promotion Agency for R&D Outcomes (COMPA) funded by the MSIT(2022RME-G01).

Declaration of competing interest

The authors declare that they have no known competing financial interests or personal relationships that could have appeared to influence the work reported in this paper.

References

[1] J.D. Steven, C. Ken, H.D. Matthews, "Future CO_2 Emissions and Climate Change from Existing Energy Infrastructure", Science. 329, pp. 1330-1333, 2010.

[2] R.B. Jackson, C.L. Quere, R.M. Andrew, J.G. Canadell, G.P. Peters, J. Roy, L. Wu, "Warning signs for stabilizing global CO_2 emissions", Environ. Res. Lett. 12, pp. 110202, 2017.

[3] B. Andersson, A. Wallin, "Students' Understanding of the Greenhouse Effect, the Societal Consequences of Reducing CO_2 Emissions and the Problem of Ozone Layer Depletion", J. Res. Sci. Teach, 37, pp. 1096-1111, 2000.

[4] World Nuclear Association, "Climate change-The science", 2021.

[5] A.M. Abdalla, S. Hossain, A.T. Azad, P.M.I. Petra, F. Begum, G. Eriksson, A.K. Azad, "Nanomaterials for solid oxide fuel cells: a review. Renew", Sustain. Energy Rev. 82, pp. 353-368, 2018.

[6] K.E. Song, S.H. Woo, S.W. Baek, H. Kang, W.S. Choi, J.Y. Park, J.H. Kim, "$_{SmBa1-x}Ca_xCo_2O_{5+d}$ Layered Perovskite Cathodes for Intermediate Temperature-operating Solid Oxide Fuel Cells", Front. Chem, 8, pp. 628813, 2021.

[7] R. Gilltae, H. Kim, H. Jeon, K. Yoon, "Fuel Consumption and CO_2 Emission Reductions of Ships Powered by a Fuel-Cell-Based Hybrid Power Source", J. Mar. Sci. Eng, 7, pp. 230, 2019.

[8] H. Koide, Y. Someya, T. Yoshida, T. Maruyama, "Properties of Ni/YSZ cermet as anode for SOFC", Solid State Ion. 132(3-4), pp. 253-260, 2000.

[9] S.B. Jin, K.S. Kim, S.W. Baek, H.S. Kim, H.I. Kang, W.S. Choi, J.H. Kim, “Characterization of layered perovskite nanofibers using electrospinning for cathode materials of low temperature-operating solid oxide fuel cell”, New. Renew. Energy, 13(2), pp. 50-58, 2017.

[10] L. Zhao, J. Drennan, C. Kong, S. Amarasinghe, S. Jiang, “Insight into surface segregation and chromium deposition on $La_{0.6}Sr_{0.4}Co_{0.2}Fe_{0.8}O_{3-d}$ cathodes of solid oxide fuel cells”, J. Mater. Chem. A, 2, pp. 11114-11123, 2014.

[11] P. Kofstad, R. Bredesen, “High temperature corrosion in SOFC environments”, Solid State ion, 52, pp. 425-443, 1992.

[12] J.W. Fergus. “Effect of cathode and electrolyte transport properties on chromium poisoning in solid oxide fuel cells”, Int. J. Hydrog, 32, pp. 3664-3671, 2007.

[13] S. Nina, B. Edith, E. Andreas, K. Patrice, T. Christian, H. Till, S. Werner, “Long-term stability of the IT-SOFC cathode materials $La_{0.6}Sr_{0.4}CoO_{3-d}$ and La_2NiO_{4+d} against combined chromium and silicon poisoning”, Solid State ion, 276, pp. 62-71, 2015.

[14] S.W. Song, S.W. Choi, H. Kang, S.W. Baek, A.K. Azad, J.Y. Park, J.H. Kim, “Synthesis and electrochemical properties of layered perovskite substituted with heterogeneous lanthanides for intermediate temperature-operating solid oxide fuel cell”, Int. J. Hydrog, 43(24), pp. 11378-11385, 2018.

[15] J. Molenda, K. Swierczek, C.W. Zaja, ”Functional materials for the IT-SOFC”, J Power Sources, 173, pp. 657-670, 2007.

[16] E. Fabbri, L. Bi, D. Pergolesi, E. Traversa, “Towards the next generation of solid oxide fuel cells operating below 600 ^{o}C with chemically stable proton-conducting electrolytes”, Adv

Mater, 24, pp. 195-208, 2012.

[17] J.H. Kim, “Electrochemical Investigation in Particle Size and Thermal Cycles of Sr Doped Layered Perovskite Based Composite Cathodes for Intermediate Temperature-operating Solid Oxide Fuel Cell”, J. Korean Electrochem. Soc, 14, pp. 176-183, 2011.

[18] S.H. Woo, T.H. Shin, H. Kang, W.S. Choi, H.S. Kim, J.H. Kim, “Phase synthesis and electrochemical characteristics of non-stoichiometric Sm1-xBa0.5Sr0.5Co2O5+d layered perovskites for IT-SOFC cathodes”, New. Renew. Energy, 6 (15), pp. 81-89, 2019.

[19] K.E. Song, H. Schlegl, C.G. Kim, K.S. Baek, Y.R. Lim, J.H. Nam, H.S. Kim, J.H. Kim, “Electrical conductivity properties of porous $SmBaCo_2O_{5+d}$ and $SmBa_{0.5}Sr_{0.5}Co_2O_{5+d}$ layered perovskite oxide systems for solid oxide fuel cell”, Ceram. Int, 2020.

[20] A. Cros, “Charging effects in X-ray photoelectron spectroscopy”, J. Electron Spectrosc. Relat. Phenom., 59, pp. 1-14, 1992.

[21] J.H. Kim, Y.M. Kim, A.C. Paul, T.S.I. John, J.M. Bae, Z. Wuzong, “Structural, thermal and electrochemical properties of layered perovskite $SmBaCo_2O_{5+d}$, a potential cathode material for intermediate-temperature solid oxide fuel cells”, J. Power Sources, 194, pp. 704-711, 2009.

[22] J.H. Kim, M. Cassidy, J.T.S. Irvine, J.M. Bae, “Advanced electrochemical properties of $LnBa_{0.5}Sr_{0.5}Co_2O_{5+d}$ (Ln = Pr, Sm, and Gd) as Cathode Materials for IT-SOFC”, J. Electrochem. Soc, 156, pp. B682, 2009.

[23] T.V. Aksenova, L.Y. Gavrilova, A.A. Yaremchenko, V.A. Cherepanov, V.V. Kharton, “Oxygen nonstoichiometry, thermal expansion and high-temperature electrical properties of layered $NdBaCo_2O_{5+d}$ and $SmBaCo_2O_{5+d}$”, Mater Res Bull. 45(9), pp. 1288-1292, 2010.

[24] J. M. Jerez, J.P. Matinez, P. Nunez, “Study of the oxygen desorption from $GdBa_{1-x}Sr_xCo_2O_{5+\delta}$ (x = 0, 0.25, 0.5 and 1): Effect of the Sr-content on the oxidation state of cobalt ions”, J. Alloys Compd, 606(5), pp. 269-272, 2014.

[25] L.H. Ahrens, “The use of ionization potentials Part 1. Ionic radii of the elements”, Geochim. Cosmochim. Acta. 2, pp. 155-169. 1952.

[26] L. Pauling, “The Nature of the Chemical Bond”, J. Am. Chem. Soc. 53(4), pp. 1367–1400, 1931.

[27] J.H. Kim, A. Manthiram, “$LnBaCo_2O_{5+d}$ perovskite cathodes for solid oxide fuel cells: and overview and perspective”, J. Mater. Chem. A. 3, pp. 24195-24210, 2015.

[28] B.C.H. Steele, "Survey of materials selection for ceramic fuel cells II. Cathodes and anodes”, Solid State Ion., 86-88, pp. 1223-1234, 1996.

[29] S.W. Baek, A.K. Azad, J.T.S. Irvine, W.S. Choi, H.I. Kang, J.H. Kim, “Electrochemical properties of composite cathodes using Sm doped layered perovskite for intermediate temperature-operating solid oxide fuel cell”, Appl. Surf. Sci, 432, pp. 272-277 2018.

[30] Z. Ling, N. Qiong, H. Beibei, L. Bin, “Novel layered perovskite oxide $PrBaCuCoO_{5+d}$ as a potential cathode for intermediate-temperature solid oxide fuel cells”, J. Power Sources, 195, pp. 453-456, 2010.

[31] K.E. Song, S.H. Woo, S.W. Baek, H.I. Kang, W.S. Choi, J.Y. Park, J.H. Kim, “$SmBa_{1-x}Ca_xCo_2O_{5+d}$ Layered Perovskite Cathodes for Intermediate Temperature-operating Solid Oxide Fuel Cells”, Front Chem, 8, pp. 628823, 2021.

[32] L.W. Tai, M.M. Nasrallah, H.U. Anderson, D.M. Sparlin, S.R. Sehlin, “Structure and electrical properties of $La_{1-x}Sr_xCo_{1-y}Fe_yO_3$. Part 1. The system $La_{0.8}Sr_{0.2}Co_{1-y}Fe_yO_3$”, Solid

State Ion., 76, pp. 259-271, 1995.

[33] Y. Kim, H. Schlegl, K. Kim, J.T.S. Irvine, J.H. Kim, “X-ray photoelectron spectroscopy of Sm-doped layered perovskite for intermediate temperature-operating solid oxide fuel cell”, Appl. Surf. Sci., 288(1), pp. 695-701, 2014.

[34] A. Subardi, C.C. Chen, M.H. Cheng, W.K. chang, Y.P. Fu, “Electrical, thermal and electrochemical properties of $SmBa_{1-x}Sr_xCo_2O_{5+\delta}$ cathode materials for intermediate-temperature solid oxide fuel cells”, Electrochim. Acta, 204, pp. 118-127, 2016.

[35] B.J. Tan, K.J. Klabunde, P.M.A. Sherwood, “XPS studies of solvated metal atom dispersed (SMAD) catalysts. Evidence for layered cobalt-manganese particles on alumina and silica”, J. Am. Chem. Soc, 113(3), pp. 855-861, 1991.

[36] T. Nitadori, M. Muramatsu, M. Misono, “Oxydation of carbon monoxide on $LaMn_{1-x}Cu_xO_3$ perovskite-type mixed oxides”, Chem. Mater, 90, pp. 1183-1189, 1994

[37] J.H. Kim, A. Manthiram, “Layered $LnBaCo_2O_{5+d}$ perovskite cathodes for solid oxide fuel cells: an overview and perspective”, J. Mater. Chem. A., 48, pp. 24195-24210, 2015.

[38] J.H. Kim, J.T.S. Irvine, “Characterization of layered perovskite oxides $NdBa_{1-x}Sr_xCo_2O_{5+\delta}$ (x = 0 and 0.5) as cathode materials for IT-SOFC”, Int. J. Hydrog. Energy., 37(7), pp. 5920-5929, 2012.

[39] F.S. Baumann, J. Fleig, H.U. Habermeier, J. Maier, "$Ba_{0.5}Sr_{0.5}Co_{0.8}Fe_{0.2}O_{3-d}$ thin film microelectrodes investigated by impedance spectroscopy”, Solid State Ion, 177, pp. 3187-3791, 2006.

[40] M.J. Jorgensen, M. Mogensen, ‘‘Impedance of solid oxide fuel cell LSM/YSZ composite

cathodes", J. Electrochem. Soc., 148, pp. A433-A442, 2001.

[41] J.H. Kim, M. Cassidy, J.T.S. Irvine, J.M. Bae, "Electrochemical investigation of composite cathodes with $SmBa_{0.5}Sr_{0.5}Co_2O_{5+d}$ cathodes for intermediate temperature-operating solid oxide fuel cell", Chem. Mater, 22, pp. 883-892, 2010.

[42] M. Li, W. Zhou, M. Zhao, Z. Zhu, "A comparative study of $SrCo_{0.8}Nb_{0.2}O_{3-\delta}$ and $SrCo_{0.8}Ta_{0.2}O_{3-\delta}$ as low-temperature solid oxide fuel cell cathodes: effect of non-geometry factors on the oxygen reduction reaction", J. Mater. Chem. A., 3, pp. 24064-24070, 2015.

[43] D. Chaudhuri, P.W. Menezes, D.D. Sarma, "Remarkable thermal stability of BF3-doped polyaniline", Appl. Phys. Lett. 83, pp. 2348-2350, 2003.

[44] S. Kim, Y.L. Yang, R. Christoffersen, A.J. Jacobson, "Oxygen permeation, electrical conductivity and stability of the perovskite oxide $La_{0.2}Sr_{0.8}Cu_{0.4}Co_{0.6}O_{3-x}$", Solid State Ion, 104, pp. 57-65, 1997.

[45] A. Aguadero, D. Pérez-Coll, J.A. Alonso, S.J. Skinner, J. Kilner, "A New Family of Mo-Doped $SrCoO_{3-\delta}$ Perovskites for Application in Reversible Solid State Electrochemical Cells", Chemistry of materials, 24, pp. 2655-2663, 2012.

[46] J.H. Chan, J.A. Bock, H. Guo, T.M. Susan, C.A. Randall, "High-temperature thermoelectric characterization of filled strontium barium niobates: power factors and carrier concentrations", J. Mater. Res. 32, pp. 1160-1167, 2017.

[47] K.E. Song, J.W. Lee, Y.R. Lim, S.W. Baek, T.H. Shin, S.K. Lee, H. Schlegl, J.H. Kim, "Influence of microstructure and applied current on the electrical conductivity of $SmBaCo_2O_{5+d}$ cathode in solid oxide fuel cell", Int. J. Hydrog. Energy, 47(35), pp. 15875-15886, 2022.

[48] K.S. Baek, S.W. Baek, H.I. Kang, W.S. Choi, J.Y. Park, S. Saxin, S.K. Lee, J.H. Kim, "Electrical conductivity characteristics of Sr substituted layered perovskite cathode ($SmBa_{0.5}Sr_{0.5}Co_2O_{5+d}$) for intermediate temperature-operating solid oxide fuel cell", 48(11), pp. 15770-15779, 2022.

[49] J.S. Park, H.G. Kim, "Electrical Conductivity and Defect Models of MgO-Doped Cr_2O_3", J. Am. Ceram. Soc, 71(3), pp. 173-176, 1988.

[50] E. Boehm, J.M. Bassat, M.C. Steil, P. Dordor, F. Mauvy, J.C. Grenier, "Oxygen transport properties of $La_2Ni_{1-x}Cu_xO_{4+\delta}$ mixed conducting oxides", Solid State Sci, 5, pp. 973-981, 2003.

[51] H.Y. Tu, Y. Takeda, N. Imanishi, O. Yamamoto, "$Ln_{1-x}Sr_xCoO_3$ (Ln = Sm, Dy) for the electrode of solid oxide fuel cells", Solid State Ion, 100, pp. 283-288, 1997.

[52] H. Han, J.S. Lee, J.H. Ryu, K.M. Kim, J.L. Jones, J. Lim, S. Guillemet-Fritsch, J.C. Lee, S.W. Mhin, "Effect of high cobalt concentration on hopping motion in cobalt manganese spinel oxide ($Co_xMn_{3-x}O_4$, x≥2.3), J. Phys. Chem. C, 120(25), pp. 13667-13674, 2016.

[53] S. Kim, Y.L. Yang, R. Christoffersen, A.J. Jacobson, "Oxygen permeation, electrical conductivity and stability of the perovskite oxide $La_{0.2}Sr_{0.8}Cu_{0.4}Co_{0.6}O_{3-x}$", Solid State Ion, 104(1-2), pp. 57-65, 1997.

[54] R. Genouel, C. Michel, N. Nguyen, F. Studer, M. Hervieu, B. Raveau, "On the cubic Perovskites $La_{0.2}Sr_{0.8}Cu_{0.4}M_{0.6}O_{3-y}$ (M = Co, Fe)", Solid State Chem., 119, pp. 260, 1995.

[55] S. Paydar, M.H. Shariat, S. Javadpour, "Investigation on electrical conductivity of LSM/YSZ8, LSM/$Ce_{0.8}4Y_{0.16}O_{0.96}$ and LSM/$Ce_{0.42}Zr_{0.42}Y_{0.16}O_{0.96}$ composite cathodes of SOFCs", Int J Hydrog Energy. 41, pp. 23145–23155, 2016.

[56] A.A. Samat, A.A. Jais, M.R. Somalu, N. Osman, A. Muchtar, K.L. Lim, “Electrical and electrochemical characteristics of $La_{0.6}Sr_{0.4}CoO_{3-\delta}$ cathode materials synthesized by a modified citrate-EDTA sol-gel method assisted with activated carbon for proton-conducting solid oxide fuel cell application”, J. Sol Gel. Sci. Tec, 86, pp. 617-630, 2018.

[57] H.E. Khal, A. Cordier, N. Batis, E. Siebert, S. Georges, M.C. Steil, “Effect of porosity on the electrical conductivity of LAMOX materials”, Solid State Ion, 304, pp. 75-84, 2017.

[58] K.Y. Park, J.M. Lim, N.S. Luu, J.R. Downing, S.G. Wallace, L.E. Chaney, H. Yoo, W.J. Hyun, H. Kim, M.C. Hersam, “Concurrently Approaching Volumetric and Specific Capacity Limits of Lithium Battery Cathodes via Conformal Pickering Emulsion Graphene Coatings”, Adv. Energy Mater., 10, 2020.

[59] N. Nakagawa, H. Sagara, K. Kato, “Catalytic activity of Ni–YSZ–CeO_2 anode for the steam reforming of methane in a direct internal-reforming solid oxide fuel cell”, J. Power Sources, 92(1), pp. 88-94, 2001.

[60] N.Q. Minh, “Cell and stack design, fabrication and performance”, High-Temperature Solid Oxide Fuel Cells for the 21st Century (Second Edition), 255-282, 2016.

[61] K. Yi, L. Sun, Q. Li, T. Xia, L. Huo, H. Zhao, J. Li, Z. Lu, J.M. Bassat, A. Rougier, S. Fourcade, J.C. Grenier, “Effect of Nd-deficiency on electrochemical properties of $NdBaCo_2O_{6-\delta}$ cathode for intermediate-temperature solid oxide fuel cells”, Int. J. Hydrog. Energy, 41(24), pp. 10228-10238, 2016.